NASA Contractor Report 3289

Computational Models for the Viscous/Inviscid Analysis of Jet Aircraft Exhaust Plumes

Sanford M. Dash, Harold S. Pergament,
and Roger D. Thorpe

CONTRACT NAS1-14794
MAY 1980

NASA

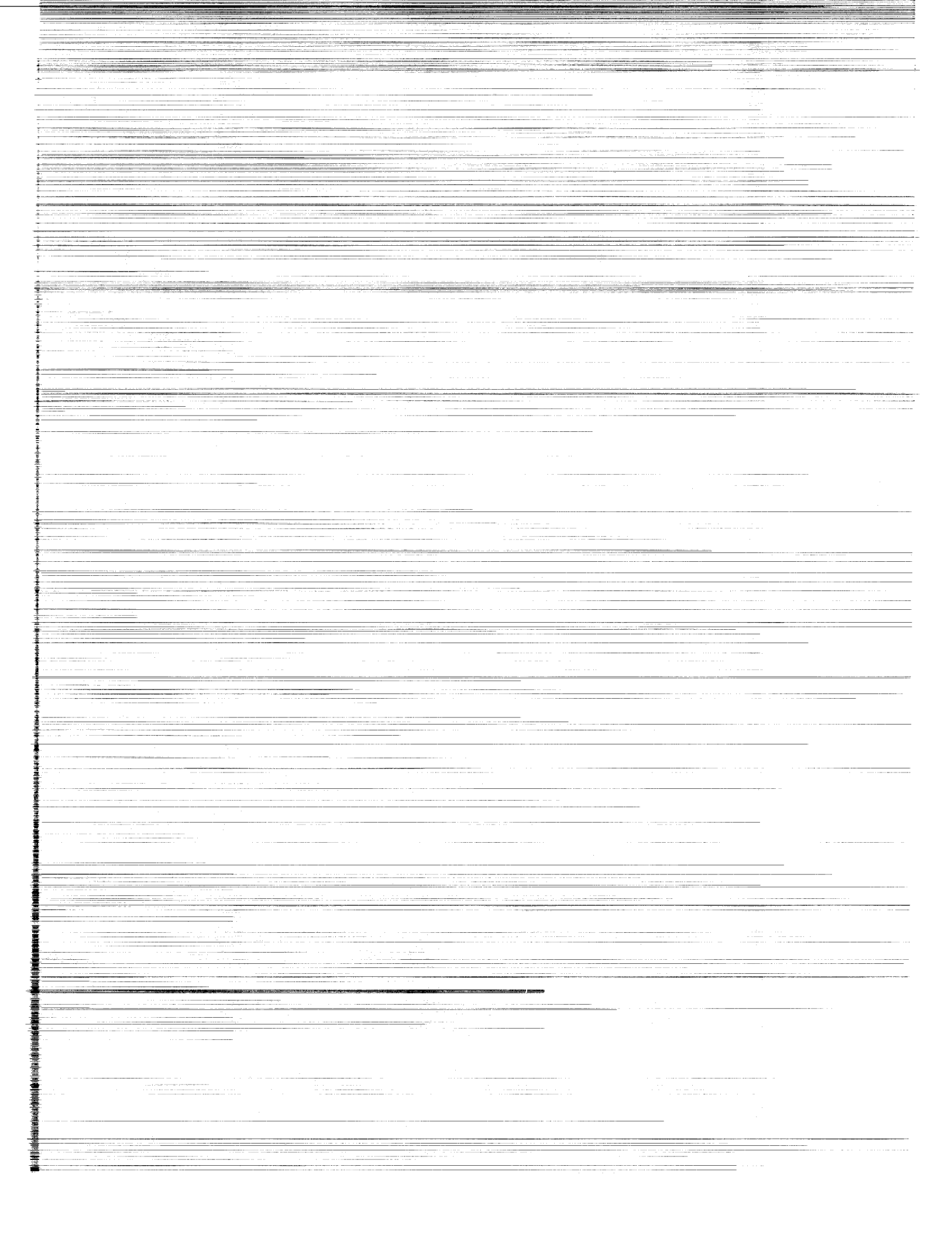

NASA Contractor Report 3289

Computational Models for the Viscous/Inviscid Analysis of Jet Aircraft Exhaust Plumes

Sanford M. Dash, Harold S. Pergament,
and Roger D. Thorpe
Aeronautical Research Associates of Princeton, Inc.
Princeton, New Jersey

Prepared for
Langley Research Center
under Contract NAS1-14794

National Aeronautics
and Space Administration

**Scientific and Technical
Information Office**

1980

FOREWORD

This document comprises the final report for Contract No. NAS1-14794, covering the period February 14, 1977 to September 30, 1979. The principal accomplishments achieved under this contract include:

(1) the development of the BOAT code which analyzes turbulent mixing processes in a variable pressure field, employing a new overlaid procedure;

(2) the formulation of a viscous/inviscid interaction model which determines the "effective" plume boundary in accordance with the jet entrainment prediction of BOAT, and;

(3) the development of the SCIPAC aircraft plume code, derived from the generalized shock capturing model, SCIPPY.

This contract was monitored by Richard G. Wilmoth who shared in the formulation of the interaction model, and has incorporated the BOAT and SCIPAC codes into an existing NASA/LRC model for predicting afterbody drag. The assistance of Ms. Shelley Abuchowski of A.R.A.P. in programming the BOAT and SCIPPY codes is gratefully acknowledged.

Additional documentation describing the research performed under this contract includes:

(a) Ref. 6
(b) Ref. 7
(c) Ref. 8
(d) Ref. 9
(e) Ref. 1
(f) Ref. 2

Refs. (a) - (d) provide a detailed description of the original BOAT code and its performance in analyzing a variety of problems. Refs. (e) - (f) describe the NASA/LRC patched model and its performance in predicting the interactive effects of jet entrainment on afterbody drag. This final report concentrates upon a description of the BOATAC and BOATAB codes (which are updated and more specialized versions of the original BOAT code), and, the SCIPAC code.

TABLE OF CONTENTS

FOREWORD....iii

LIST OF FIGURES....vi

NOMENCLATURE....vii

1. SUMMARY....1

2. INTRODUCTION....1

3. PREDICTION OF JET INVISCID STRUCTURE....3

3.1 Methodology....3

3.2 Governing Equations....4

3.3 Real Gas Thermodynamics....6

3.4 Integration Procedure and Decode....7

1. Interior Point Integration....7

2. Decode Procedure....8

3. Boundary Point Procedure....10

3.5 Mach Disc Methodology....11

1. Approach....11

2. Triple Point Procedure....11

3. Shock Jump Procedure....11

4. Automated Mach Disc Location Procedure....12

5. Regular Reflection and Sting Default Options....14

6. Integration Procedure....15

7. Low Mach Number Default Option....16

3.6 Sample Calculations....17

4. OVERLAID ANALYSIS OF TURBULENT MIXING AND AFTER-BURNING PROCESSES....18

4.1 Methodology....18

4.2 Governing Equations....19

4.3 Computational Scheme....21

4.4 Computational Boundary Growth....22

4.5 Redistribution of Grid Points....24

4.6 Temperature Inversion....25

4.7 Integration Procedure....26
4.8 Treatment of Finite Rate Chemistry....26
4.9 Initialization Options....29
4.10 Effective Plume Geometry....30
4.11 Calculations....31
5. CODE/SUBROUTINE DESCRIPTIONS....32
5.1 SCIPAC....32
5.2 BOATAC and BOATAB....34
6. CONCLUDING REMARKS....36
APPENDIX I - INPUT INSTRUCTIONS FOR SCIPAC....37
APPENDIX II - INPUT INSTRUCTIONS FOR BOATAC/AB....40
REFERENCES....47
TABLE 1....50
FIGURES....51

TABLE

Table 1. Summary of constant pressure, turbulent shear flow comparisons of BOAT Predictions with Laboratory Data....50

LIST OF FIGURES

1. Schematic of afterbody/exhaust flowfield....51
2. Inviscid exhaust plume structure....52
3. Characteristic nomenclature at boundary points....53
4. Mach disc nomenclature....54
5. Pressure and normal velocity profiles showing captured barrel shock....55
6. Flowfield schematic of underexpanded hot air jet and predicted centerline pressure and Mach number variation....56

7.A Profiles of P, V, T and M at X/r_j = 1.16.....57
7.B Profiles at 2.17.....58
7.C Profiles at 2.67.....59
7.D Profiles at 3.35, upstream of Mach disc.....60
7.E Profiles at 3.35, downstream of Mach disc.....61
8. Axial variations of Mach number, slipstream angle and streamtube size for several trial Mach disc locations.....62
9. Comparison of several techniques for getting through the throat.....63
10. Multiple cell inviscid pattern for slightly overexpanded plume exhausting into still air.....64
11. Mixing solution overlaid on inviscid flowfield maps.....65
12. Computational network of BOAT.....66
13. SCIPAC subroutine flowchart.....67
14. BOATAC subroutine flowchart.....68
15. BOATAB subroutine flowchart.....69

NOMENCLATURE

a_i	coefficients for thermodynamic curve fits
b_i	coefficients for low temperature thermodynamic curve fits
C_p	specific heat at constant pressure
C_μ	coefficient in expression for μ_t in kε model
$C_{1,2}$	coefficients in ε equation
e_k	conservation variables in E vector array
E,F,G	vector arrays in SCIPAC defined in Equation (1)
$F\pm$	forcing function in characteristic compatibility relation (Equation (7))
F_i	α_i/W
f,g	vector arrays in BOAT defined in Equation (31)

h_i	static enthalpy of species i
h	static enthalpy of mixture
H	total enthalpy of mixture
k	turbulent kinetic energy
ℓ	length scale for Prandtl mixing length model
M	Mach number
P_r	turbulent Prandtl number
P	pressure, also production term in k equation
Q	magnitude of inviscid velocity
R	universal gas constant
r,R	radial coordinate
r_c	radial coordinate of inviscid plume interface
r_{eff}	radial coordinate of effective plume boundary
T	temperature
U	inviscid velocity component in axial direction
u	viscous velocity component in axial direction
V	inviscid velocity component in radial direction
v	viscous velocity component in radial direction
W	mixture molecular weight
$\dot{w}$	chemical source term
x,X	axial coordinate
α_i	mole fraction of i^{th} species
γ	specific heat ratio
ε	turbulent dissipation rate

ξ,η	mapped coordinates in SCIPAC
ρ	density
$\lambda\pm$	characteristic directions
δ	viscous layer radial extent
δ^*	displacement thickness of viscous layer
θ	flow deflection angle
σ	effective Prandtl number array in Equation (31)
σ_o	spread rate parameter with one stream stationary
μ	Mach angle
μ_t	turbulent viscosity
ψ	streamfunction

1. SUMMARY

Computational models which analyze viscous/inviscid flow processes in jet aircraft exhaust plumes are discussed. These models are component parts of the NASA/LRC system for the prediction of nozzle afterbody drag.[1,2] Inviscid/shock processes are analyzed by the SCIPAC code which is a compact aircraft version of the generalized SCIPPY model.[3-5] SCIPAC analyzes underexpanded jet exhaust gas mixtures (of hydrocarbon exhaust products and air) via a shock capturing methodology. A detailed and automated treatment of the embedded subsonic zones behind Mach discs is provided for in this analysis. Mixing processes along the plume interface are analyzed by two upgraded versions of the original BOAT code.[6,7] BOATAC is a frozen chemistry version of BOAT containing the same aircraft thermodynamic package as SCIPAC. BOATAB is an afterburning version with a self-contained aircraft (hydrocarbon/air) finite-rate chemistry package. The coupling of viscous and inviscid flow processes is achieved by an overlaid procedure[8,9] with interactive effects accounted for by a displacement thickness type correction to the inviscid plume interface.

2. INTRODUCTION

In the NASA/LRC system for predicting boattail drag,[1,2] the various regions of the afterbody/exhaust flowfield (Fig. 1) are separately analyzed. The overall flowfield solution is arrived at by patching these regional solutions together in the iterative manner discussed in Refs. 1 and 2. Plume induced effects are included in this methodology via the prediction of the detailed inviscid plume flow pattern, the "overlaid" analysis of turbulent mixing processes along the plume interface and, the determination of the "effective" plume geometry via a displacement thickness type correction to the inviscid plume interface.

The inviscid flow pattern is calculated by SCIPAC which is an aircraft version of the SCIPPY code.[3-5] The generalized version of SCIPPY is a component part of the JANNAF Standardized Rocket Plume Flowfield Model * (SPF)[10,11] and contains several features not required in an aircraft exhaust plume model (viz., the treatment of gas/particle interactions,[5] the fully coupled treatment of viscous/inviscid interactions in supersonic mixing regions,[4] the analysis of the supersonic flow external to the plume,[11] and a multiple domain methodology in a choice of coordinate systems). In developing SCIPAC, the procedures in SCIPPY relevant to aircraft plumes were selectively extracted and combined into a compact code which has the following features:

---

*Under development for the JANNAF Exhaust Plume Technology Subcommittee. Monitored by U.S. Army Missile R&D Command, Redstone Arsenal, Alabama, Contract No. DAAK40-78-C-0124.

(1) Integrates the inviscid conservation equations for a uniform composition gas mixture in supersonic regions of the exhaust plume flowfield.

(2) Employs a shock-capturing methodology in mapped cylindrical coordinates.

(3) Contains an aircraft thermodynamic package for an exhaust gas mixture comprised of hydrocarbon combustion products and air.

(4) Provides for a detailed and fully automated analysis of the embedded subsonic region behind the first Mach disc.

(5) Generates a flowfield map which is supplied to the mixing model for use in the subsequent "overlaid" analysis.

The "overlaid" analysis of turbulent mixing processes along the plume interface is performed by two new, optimized versions of the BOAT code. The original version of BOAT[6-9] provided for the analysis of generalized thermochemical systems, a feature not required for aircraft exhausts. The newly developed BOATAC code is a compact, frozen chemistry version of BOAT for nonafterburning exhausts and contains the same aircraft thermodynamic package as SCIPAC. BOATAB is an afterburning version of BOATAC with a self-contained aircraft (hydrocarbon/air) chemical kinetic package.

The BOAT code is also an integral part of the JANNAF SPF.[10,11] Many improvements to the original version have been made under this rocket plume standardization effort, which have been incorporated into the BOATAC and BOATAB codes. The "new" features contained in BOATAC and BOATAB are listed below:

(a) The total enthalpy is used as the dependent variable in the energy equation in place of the temperature.

(b) Cubic polynomials are used in the property resetting procedure in place of linear interpolations.

(c) The thermodynamic data is self-contained and in the form of polynomial fits in place of tabular data.

(d) The chemical kinetic data (in BOATAB) is self-contained.

(e) The boundary layer initialization procedure is now based upon the Reshotko-Tucker analysis[12] for consistency with the model employed in the NASA/LRC system.[1,2]

(f) A separated flow initialization procedure has been provided yielding profiles at the reattachment point based on the Presz model.[13]

(g) The previously employed "entrainment" rules for estimating boundary growth have been eliminated and a new, efficient growth procedure has been implemented.

(h) The codes have been entirely restructured for computational efficiency.

In Section 3, the governing equations and computational procedures employed in SCIPAC will be summarized. A detailed description of the numerical procedures is available in Ref. 3. The discussion here will concentrate upon new features and those unique to SCIPAC, such as the Mach disc analysis and treatment of real gas effects. The equations and new computational procedures employed in the BOATAC and BOATAB codes will be summarized in Section 4. A detailed description of the features contained in the original formulation is available in Refs. 6 and 7. Descriptions of all three computer codes are provided in Section 5, while input instructions for these codes are provided in the appendices.

Nozzle afterbody drag predictions employing the original BOAT code (and, in some instances, a preliminary version of SCIPAC) have been reported in Refs. 1, 2, 6, 8, and 9. Refs. 6, 8, and 9 detail the overlaid methodology employed in coupling the BOAT and SCIPAC codes and present sensitivities to modeling parameters such as the choice of turbulence model employed in the mixing analysis.

3. PREDICTION OF JET INVISCID STRUCTURE

3.1 Methodology

The supersonic inviscid plume flowfield resulting from an underexpanded jet aircraft exhaust (Fig. 2) is solved in SCIPAC by a forward spatial marching procedure. The calculation is initiated at the nozzle exit plane with exhaust properties prescribed and the initial plume interface angle determined by locally expanding the exhaust flow at the lip to the external pressure.* The calculation is performed with a fixed number of grid intervals equally spaced between the axis and the plume interface.

---

*For the subsonic/transonic external flows of interest here, the external pressure is prescribed along the plume interface, based upon the South/Jameson relaxation solution[14] over the "effective" plume geometry in a previous iterative pass (see Refs. 1 and 2).

As the calculation proceeds downstream, the plume interface angle monotonically decreases and the resultant downrunning compression waves coalesce forming a barrel shock. The calculation proceeds in this manner until a Mach disc is dropped. The correct Mach disc (triple-point) location is not known apriori and must be iteratively determined. Downstream of the Mach disc location, points are evenly distributed between the Mach disc slipstream and the plume interface. The flow within the Mach disc streamtube is treated one-dimensionally. Oblique shocks (barrel and reflected) are numerically captured by integrating the conservation form of the inviscid equations and using the two-step difference algorithm of MacCormack.[15] At the triple-point, shock fitting procedures are employed. The calculation is terminated somewhat downstream of the Mach disc streamtube sonic throat location in the second inviscid cell, since the plume geometry downstream of the first inviscid cell has a negligible influence on nozzle afterbody pressure levels.[16]

3.2 Governing Equations

The governing inviscid equations for a uniform composition gas mixture in mapped cylindrical coordinates are given by:

$$\boxed{\frac{\partial E}{\partial \xi} + \frac{\partial F}{\partial \eta} + G = 0} \qquad (1)$$

where

$$E(k) = \begin{vmatrix} e_1 \\ e_2 \\ e_3 \\ e_4 \end{vmatrix} = \begin{vmatrix} \rho U \\ P + \rho U^2 \\ \rho UV \\ \rho UH \end{vmatrix}$$

$$F(k) = \begin{vmatrix} b\rho V - ae_1 \\ be_3 - ae_2 \\ b(P+\rho V^2) - ae_3 \\ b\rho VH - ae_4 \end{vmatrix}$$

and

$$G(k) = \begin{vmatrix} a_\eta e_1 + \rho V/r \\ a_\eta e_2 + e_3/r \\ a_\eta e_3 + \rho V^2/r \\ a_\eta e_4 + \rho VH/r \end{vmatrix}$$

The U component of velocity is in the axial (x) direction and the V component of velocity is in the radial (r) direction.

The mapping employed transforms the computational domain into a rectangular region. With the upper and lower boundaries designated by $R_U(x)$ and $R_L(x)$, the transformation to a rectangular domain is given by

$$\xi = x \tag{2a}$$

$$\eta = \frac{r - R_L(x)}{R_U(x) - R_L(x)} \tag{2b}$$

The terms a and b in Equation (1) are given by

$$a(\xi,\eta) = \frac{(1-\eta)(dR/dx)_L + \eta(dR/dx)_U}{R_U - R_L} \tag{3a}$$

$$b(\xi) = 1./(R_U - R_L) \tag{3b}$$

At the axis of symmetry, the limiting form of the equations yields

$$\frac{\partial}{\partial \xi} \begin{vmatrix} e_1 \\ e_2 \\ e_4 \end{vmatrix} + 2b \begin{vmatrix} \rho \\ \rho U \\ \rho H \end{vmatrix} \frac{\partial V}{\partial \eta} = 0 \tag{4}$$

where $e_3 = V = 0$

Other boundary points such as the plume interface and Mach disc slipstream are handled by a formal characteristic procedure in conjunction with the appropriate boundary conditions. The characteristic compatibility relations are given by

$$\frac{\sin \mu \cos \mu}{\gamma} \, d\ln P \pm d\theta + F^{\pm} dx = 0 \tag{5}$$

along the characteristic directions

$$\frac{dr}{dx} = \lambda^{\pm} = \tan(\theta \pm \mu) \tag{6}$$

The forcing function term $F^{\pm}$ is given by

$$F^{\pm} = \frac{\sin\theta \sin\mu}{r \cos(\theta \pm \mu)} \tag{7}$$

In the above relations, θ is the flow deflection angle and μ is the Mach angle.

3.3 Real Gas Thermodynamics

The exhaust composition is assumed to be uniform and comprised of the six species N_2, O_2, CO_2, H_2O, CO and CH_4.* The static enthalpy for each species, i, is given by a polynomial of the form

$$\frac{h_i(T)}{R} = a_{1_i} T + a_{2_i}\frac{T^2}{2} + a_{3_i}\frac{T^3}{3} + a_{4_i}\frac{T^4}{4} + a_{5_i}\frac{T^5}{5} + a_{6_i} \tag{8}$$

with the polynomial coefficient data extracted from Ref. 17 and built into the code. R is the universal gas constant.

The coefficient data are given in the temperature ranges of $300 < T < 1000$ K and $1000 < T < 5000$ K. Operating conditions have been extended below 300 K by inputting the values of $h_i(0)$ (obtained from the tabular data of Ref. 18) and constructing a third polynomial of the form

$$\frac{h_i(T)}{R} = \frac{h_i(0)}{R} + b_{2_i} T + b_{3_i} T^2 \tag{9}$$

where b_{2_i} and b_{3_i} are determined by requiring continuity of $h_i(T)$ and its

---

*For most aircraft exhausts, the concentrations of CO and CH_4 (included to globally represent unburnt hydrocarbons) are negligible.

derivative $C_{p_i}(T)$ at T = 300 K.

For the inviscid flows under consideration, the composition is uniform and nonchanging (frozen). For optimal efficiency, a universal static enthalpy fit is constructed by performing the following summation

$$a_K = \sum_{i=1}^{6} a_{K_i} \alpha_i \tag{10}$$

for each of the K coefficients, where α_i is the mole fraction of the i^{th} species at the nozzle exit plane. Then, the static enthalpy of the exhaust gas mixture is given by

$$\frac{h(T)}{R} = a_1 T + a_2 \frac{T^2}{2} + a_3 \frac{T^3}{3} + a_4 \frac{T^4}{4} + a_5 \frac{T^5}{5} + a_6 \tag{11}$$

and the specific heat capacity, C_p, by its derivative

$$\frac{C_p(T)}{R} = a_1 + a_2 T + a_3 T^2 + a_4 T^3 + a_5 T^4 \tag{12}$$

This summation is separately performed for the coefficients in both temperature ranges as well as for $h_i(0)$ and the b_2 and b_3 coefficients of Equation (9). The specific heat ratio, γ, is then simply given by

$$\gamma(T) = \frac{C_p(T)/R}{(C_p(T)/R)-1} \tag{13}$$

3.4 Integration Procedure and Decode

3.4.1 Interior Point Integration. For equally spaced grid intervals, $\Delta\eta$, the two-step MacCormack algorithm[15] applied to Equation (1), for the integration step, $\Delta\xi$, and the interior grid point, I, yields:*

---

*ε is alternated from 0 to 1 at each integration step to yield a nonpreferential treatment of wave propagation.
- $\varepsilon = 0$ yields forward difference predictor/backward difference corrector;
- $\varepsilon = 1$ yields backward difference predictor/forward difference corrector

Predictor Step:

$$\tilde{E}_I = E_I^k - \frac{\Delta\xi}{\Delta\eta}\left[(1-\varepsilon)F_{I+1}^k-(1-2\varepsilon)F_I^k - \varepsilon F_{I-1}^k\right] - G_I^k \Delta\xi \tag{14a}$$

Corrector Step:

$$E_I^{k+1} = \tfrac{1}{2}\left[E_I^k + \tilde{E}_I - \frac{\Delta\xi}{\Delta\eta}\left[\varepsilon\tilde{F}_{I+1}+(1-2\varepsilon)\tilde{F}_I+(\varepsilon-1)\tilde{F}_{I-1}\right] - \tilde{G}_I\Delta\xi\right] \tag{14b}$$

In the above equations, k designates properties at the station ξ, k + 1 at $\xi + \Delta\xi$ while $\sim$ designates provisional values (values based on properties determined in the predictor step). The marching step taken ($\Delta\xi$) must satisfy the CFL condition at each grid point and is determined using actual characteristic intersections (rather than a linearized procedure) as detailed in Ref. 3.

3.4.2 Decode Procedure. Between each predictor and corrector step, the physical variables U, V, P, ρ, and H must be obtained from the conservation variables, e_i, so that the vectors F and G can be constructed. V and H are readily obtained via the relations

$$V = e_3/e_1 \tag{15a}$$

and

$$H = e_4/e_1 \tag{15b}$$

while P, U, and ρ are iteratively solved via the relations,

$$P(U) = e_2 - e_1 U \tag{15c}$$

$$\rho(U) = e_1/U \tag{15d}$$

$$H = h(T) + \tfrac{1}{2}(U^2 + V^2) \tag{15e}$$

where

$$T(U) = \frac{P(U)W}{\rho(U)R} \tag{15f}$$

More than one solution branch exists* for this set of equations and great care must be taken in the iterative decode process so that one remains on the desired (weak solution) branch. Difficulties can arise in strong wave regions (i.e., traversing a captured shock) which are circumvented by good initial guesses. The procedure employed makes use of the pressures at adjacent grid points for the first two iterations. At the predictor level, values at the previous integration step are employed while at the correction level, predictor values are used. Experience has indicated that if the pressure difference at the adjacent grid points exceeds twenty percent, the first iterative guess should be taken with the maximum of these pressures and the second with a value decreased from the maximum by twenty-five percent of the pressure difference. For the third and subsequent iterations, the assumed value of pressure, $P^{(i)}$ is given by

$$P^{(i)} = P^{(i-1)} - \Delta H^{(i-1)} \frac{(P^{(i-1)} - P^{(i-2)})}{(\Delta H^{(i-1)} - \Delta H^{(i-2)})} \tag{16}$$

where i designates the iteration counter and ΔH the difference between the correct value of H (given by eq. 15b) and the value $H^{(i)}$ corresponding to the assumed pressure $P^{(i)}$ (determined via eqs. 15c-f). A maximum of 5 iterations is required in strong wave regions of the flow.

For a perfect gas, the static enthalpy is given by the relation

$$h = \frac{\gamma}{\gamma-1} \frac{P}{\rho} \tag{17}$$

which when inserted into Equation (15e) along with the expressions for P and ρ given in Equations 15c and d yields the following quadratic expression for U:

*Two of the branches are physical and correspond to weak and strong shock solutions (viz. in a wave oriented coordinate system, the solutions would represent a Mach wave and a normal shock). Nonphysical branches represent "expansion" shock and reversed flow solutions.

$$U = \frac{-B \pm (B^2 - 4AC)^{\frac{1}{2}}}{2A} \tag{18}$$

where

$$A = \frac{\gamma+1}{2\gamma}$$

$$B = -e_2/e_1$$

$$C = \frac{\gamma-1}{2\gamma}(2H-V^2)$$

The plus sign is used for the desired weak solution, while the minus sign is used in conjunction with shock jump procedures.

3.4.3 Boundary Point Procedure. At boundary points, the characteristic compatibility relations are also solved by a two-step predictor/corrector procedure whose details are available in Ref. 3. Boundary conditions are stipulated by relations of the form

$$f(P_C,\theta_C) = 0 \tag{19}$$

while the difference form of the compatibility relations along $\lambda\pm$ (See Fig. 3) is given by

$$\frac{(\sin\mu\cos\mu)}{\gamma}_{A,B}(\ln P_C - \ln P_{A,B}) \pm (\theta_C - \theta_{A,B}) + F^{\pm}_{A,B}\Delta X = 0 \tag{20}$$

Equations (19) and (20) yield the values of P_C and θ_C at the upper or lower boundary point, while the following relations yield the remaining flowfield properties.

$$\rho_C = \rho_D\,(P_C/P_D)^{1/\gamma}\ CD \tag{21}*$$

*The actual P/ρ relation employed in the code does not stipulate constancy of entropy along boundary streamlines since the entropy associated with captured shocks reflecting off boundary surfaces would then be ignored. The procedure introduced in Ref. 19 is employed wherein the entropy level at the boundary is set equal to that at the adjacent grid point (i.e., the D point is replaced by the I = 2 or IMAX-1 point in Equation 21).

$$H_C = H_D \tag{22}$$

$$Q_C = H_C - h_C\,(T_C) \tag{23}$$

where $$T_C = \frac{P_C W}{\rho_C R} \tag{24}$$

3.5 Mach Disc Methodology

3.5.1 Approach. The approach employed for locating the Mach disc and analyzing the subsonic flow in the Mach disc streamtube closely parallels that introduced by Abbett.[20] A Mach disc position is assumed and the flow downstream of this location is analyzed treating the flow in the Mach disc streamtube one-dimensionally. The "correct" location is that which allows the subsonic flow in the 1-D streamtube to accelerate smoothly through a sonic throat. Positions chosen upstream of this location result in a subsonic to subsonic transition at the throat while those chosen downstream result in choking (i.e., sonic velocity is achieved before a throat is reached). The ability of this procedure to yield realistic Mach disc locations has been amply demonstrated in previous publications[20-22] and is not addressed herein. The significant accomplishments reported here are the inclusion of a formal Mach disc methodology in the framework of a shock capturing model and the complete automation of this methodology.

3.5.2 Triple Point Procedure. To perform a Mach disc calculation in a shock capturing model, the triple-point* procedure must incorporate logic which identifies the grid points upstream and downstream of the barrel shock (points 1 and 2 of Fig. 4). This is readily accomplished by monitoring the normal velocity profile, V(r), which monotonically increases from the axis to the barrel shock and abruptly decreases across the barrel shock. Figure 5 depicts typical calculated radial profiles of the normal velocity and pressure indicating that the barrel shock position and properties upstream and downstream (points 1 and 2) are readily identified. With the properties at points 1 and 2 identified, the pressure, P_4, behind the Mach disc is obtained via a normal shock jump from state 1. Then, an iterative procedure is initiated wherein the reflected shock angle is varied until the pressure jump from state 2 to 3 yields $P_3 = P_4$.

3.5.3 Shock Jump Procedure. The shock jumps required in the triple-point calculation are performed assuming the composition to be frozen across the shock wave. For the Mach disc calculation, the E vector array at the triple-point is in a shock-oriented coordinate system, since the U velocity

*The triple-point occurs at the juncture of the barrel shock, Mach disc and reflected shock as illustrated in Fig. 4.

component is normal to the Mach disc. Properties downstream of the Mach disc are determined by the standard real gas decode procedure of Section 3.4.2. To obtain the desired shock jump (rather than the weak) solution, initial pressure guesses are required in the vicinity of the correct shock solution. These are given by the perfect gas jump relation

$$P_4/P_1 = \frac{2\gamma M_{n_1}^2 - (\gamma-1)}{\gamma+1} \tag{25}$$

where $M_{n_1} = U_1/(\gamma P_1/\rho_1)^{\frac{1}{2}}$.

The first pressure guess is determined using $\gamma=\gamma_1$ and the second using $\gamma=\gamma_4$. Subsequent guesses employ the standard linear error extrapolation procedure given by Equation (16).

For the reflected shock calculation, P_3 is set equal to P_4 and the reflected shock angle, σ, is iteratively varied to yield $H_{T_3} = H_{T_2}$ where

$$U_{n_3} = (P_2-P_3+\rho_2 Q_2^2 \sin^2\sigma)/(\rho_2 Q_2 \sin\sigma) \tag{26a}$$

$$U_{t_3} = Q_2 \cos\sigma \tag{26b}$$

$$\rho_3 = \rho_2 Q_2 \sin\sigma/U_{n_3} \tag{26c}$$

and

$$H_{T_3} = h_3 (T_3) + .5 (U_{n_3}^2 + U_{t_3}^2) \tag{26d}$$

where T_3 is determined from the equation of state (Equation 24) using the values of ρ_3 and P_3.

3.5.4 Automated Mach Disc Location Procedure. The automation of the Mach disc methodology involves: (a) selecting a first trial location, $X_{md}(1)$, that is upstream of the "correct" location, (b) storing the flowfield data at that station on disc A, (c) advancing the solution downstream until a subsonic/subsonic transition (or rapid streamtube divergence) is detected, (d) restarting the calculation at $X_{md}(1)$ by reading the data from

disc A, (e) dropping the next Mach disc at $X_{md}(2) = X_{md}(1) + \Delta X$ and saving the data at $X_{md}(2)$ on disc B, (f) advancing the solution until *either* a subsonic/subsonic transition is detected or the flow in the Mach disc streamtube has accelerated to a Mach number of .7. If subsonic/subsonic transition is encountered, the calculation is restarted at $X_{md}(2)$ by reading data from disc B. The next Mach disc is dropped at $X_{md}(3) = X_{md}(2) + \Delta X$ with the data $X_{md}(3)$ stored on disc A. This process continues until a solution reaching M = .7 is encountered.

On reaching M = .7, the following decision process is employed:

(a) If the Mach disc slipstream has inflected prior to reaching M = .7 (see Fig. 2), the present solution is "forced" through a sonic throat by replacing the Mach disc slipstream downstream of this position with the parabola

$$r = \tilde{r} + \tan \overset{\sim}{\theta}\,(X-\tilde{X}) + \frac{\tan^2 \overset{\sim}{\theta}}{4(r-r^*)}\,(X-\tilde{X})^2 \qquad (27)$$

where $\sim$ designates the M = .7 point and r* is the sonic throat radius. This parabola is continuous with the Mach disc slipstream (in radial height and slope) at the $\sim$ point and passes through a sonic throat at the location

$$X^* = \tilde{X} + \frac{2\,(r^*-\tilde{r})}{\tan \overset{\sim}{\theta}} \qquad (28)$$

(b) If the Mach disc slipstream has not inflected prior to reaching M = .7, the present solution branch is a choked one and cannot be "forced" through a sonic throat. The correct solution lies in between the present one and the previous subsonic/subsonic solution, separated by the single integration step, ΔX. Rather than divide this interval into a subset of smaller intervals (which would deteriorate the quality of the captured barrel shock) the following procedure is followed:

(1) The Mach disc location and size is fixed at the values obtained in the previous subsonic/subsonic solution.

(2) The triple-point solution at this station is per-

turbed by decreasing the flow angle, θ_1, (see Fig. 4) in small increments.

(3) For each increment, a trial solution is performed.

(4) Each trial solution is terminated when a subsonic/subsonic transition is detected.

(5) In this sequential angle decreasing procedure, a solution will be obtained which accelerates to M = .7 (and which also inflects prior to reaching this point). This solution is "forced" through the throat using Equation (27).

It has been found that this approach is straightforward to implement in an automated fashion and yields a reasonable streamtube variation in the "parabolic" region (i.e., downstream of M = .7). In contrast, the approach suggested by Salas[22] (which involves the use of a linearized P-θ relation in the throat region) may fail if initiated on a choking branch and can yield significant errors in throat radius when initiated on a branch which has undergone inflection.

3.5.5 Regular Reflection and Sting Default Options. The first Mach disc is dropped when the triple-point solution yields a slipstream angle less than 15°*. For slightly underexpanded plumes with small nozzle lip angles, this criterion may never be met since the nonlinear strengthening of the barrel shock in approaching the axis may occur over a transverse length scale comparable to a grid interval. A regular reflection default option handles this situation. A cylindrical sting (whose radius equals one grid interval) is inserted into the flow when the barrel shock reaches the second grid point and the 15° criterion has not yet been met. This same default is employed in performing the sequence of events entailed in the automated Abbett procedure whenever the barrel shock reaches the second grid point (the slipstream angle there would be less than 15° but greater than 0°, as per the discussion in the paragraph below). The angle of the reflected shock for this default situation is determined such as to yield θ_3=0 (See Fig. 4).

An alternative "sting" default option is implemented when the triple-point solution first yields a negative slipstream angle, yet previous (positive angle) trial solutions have all resulted in subsonic/subsonic transitions at the throat location. For this situation, a cylindrical sting is

*It has been observed that this criterion generally places the first trial position upstream of the "correct" location. More precise criterion can be implemented on the basis of further numerical experimentation.

inserted into the flow whose radius is that of the triple-point. Here, the pressure, P_3, behind the reflected shock equals that behind the Mach disc, P_4. This default precludes attempts to employ the Abbett procedure for negative initial slipstream angles.*

The sting option can also be implemented as a user specified option when it is known, apriori, that Mach disc sizes will be relatively small. Then, no trial solutions will be performed and the Mach disc will be dropped at the station satisfying the sting criterion ($P_3 = P_4$, $\theta_3 \leq 0$). If the barrel shock reaches the second grid point and the sting criterion has not yet been met, the regular reflection default option will be implemented.

3.5.6 Integration Procedure. In proceeding downstream of the Mach disc location, the supersonic flow grid points are redistributed between the Mach disc slipstream and the plume interface. In either of the default options, the lower boundary is a solid cylindrical sting. In the Abbett Mach disc procedure, the following relations govern the 1-D flow in the Mach disc streamtube:

$$d\ln\rho = \frac{1}{\gamma} d\ln P \tag{29a}$$

$$dH = 0 \tag{29b}$$

$$d(\rho Q r^2) = 0 \tag{29c}$$

In the integration step, ΔX, an iterative procedure is employed to simultaneously satisfy the above relations and the characteristic compatibility relation for a lower boundary point (Fig. 3). For an assumed value of pressure, P_C, solution of the above equations in conjunction with the equation of state and real gas enthalpy fit yields all properties in the Mach disc streamtube. Two values of slipstream angle, θ_C, result from P_C:

$$\theta_C^{(1)} = \tan^{-1}\left[\frac{r_C - r_D}{\Delta X/2} - \tan\theta_D\right] \tag{30a}$$

from the Mach disc streamtube solution, and,

---

*Negative slipstream angles are generally associated with smaller size Mach discs for which the inviscid Abbett procedure tends to be inadequate. For small discs, the effects of turbulent mixing in accelerating the flow in the Mach disc streamtube can be appreciable, as discussed in Ref. 23.

$$\theta_C^{(2)} = \theta_B + \frac{(\sin \mu \cos \mu)}{\gamma}_{BC}(\ln P_C - \ln P_B) + \bar{F}_{BC}\Delta X \qquad (30b)$$

from the characteristic solution. The iteration process converges on a pressure, P_C, such that $\theta_C^{(1)} = \theta_C^{(2)}$.

The integration process is continued until one of the following situations occurs:

(1) Rapid divergence of the Mach disc streamtube occurs as detected by either $\theta_{MD} > 35°$ or $M_{MD} < .08$. This is associated with dropping a trial Mach disc well upstream of the actual location.

(2) A subsonic to subsonic transition occurs as detected by the occurrence of a minimum area in the Mach disc streamtube with a subsonic Mach number.

(3) The flow in the Mach disc streamtube accelerates to $M_{MD} \sim .7$.

If (1) or (2) occurs, the present solution is terminated and the calculation is restarted with the assumed Mach disc location shifted downstream by one integration step. If (3) occurs, the decision process discussed in Section 3.5.4 is employed.

3.5.7 Low Mach Number Default Option. For near sonic exhausts at very low pressure ratios, the Mach disc size will generally be quite small, and, the Mach number behind the reflected shock will be close to unity. In such situations, the flow downstream of the Mach disc location is solved in a simplified fashion. The approach taken involves:

(1) estimating the length of the first inviscid cell (simple geometric considerations employing the average Mach angle of the uprunning characteristic from the triple-point and the lateral extent of the plume expanded to ambient pressure yield this length)

(2) imposing an exponential variation for the pressure along each grid line from its value at the Mach disc station to the ambient pressure

(3) calculating flow properties along each grid line isentropically based on the imposed pressure variation

(4) determining the radial position of each grid point by preserving the mass flux between grid points (i.e., $\psi(I)$) for each grid point I is maintained at its value at the

Mach disc station).

The details of this "decay" procedure are available in Ref. (3). Its validity in yielding reasonable plume boundary shapes has been established by comparisons with complete numerical solutions (see Ref. (1)).

3.6 Sample Calculations

The first test case chosen was that of an underexpanded hot air jet (M_j = 1.09, T_j = 1100 K) exhausting into still air (P_j/P_∞ = 4). The calculation was performed using 41 radial grid points, the real gas thermodynamic option and the automated Mach disc procedure. A flowfield schematic is given in Fig. 6 indicating the principal wave and contact surface locations. The predicted variations of pressure and Mach number along the plume centerline are also presented in Fig. 6. The calculation was terminated at the sonic throat of the Mach disc streamtube.

Profiles of the flowfield variables P, V, T, and M at the axial stations X/r_j = 1.16, 2.17, 2.67, and 3.35 are depicted in Figs. 7A-E, respectively. At X/r_j = 1.16, a portion of the lip expansion fan has reached and reflected from the centerline, and, the barrel shock has started to form (spread over the interval $1.1 < r/r_j < 1.25$). At X/r_j = 2.17, the captured barrel shock ($r/r_j \sim 1.1$) is quite sharply defined and has a strength (P_2/P_1) of about 3. The normal velocity profile has now become linear in the core region. At X = 2.67, the strength of the barrel shock has increased and the flow angle downstream of the barrel shock has become zero (i.e., parallel to the axis).

Downstream of this location, flow angles behind the barrel shock will be negative, signaling a call to the triple-point subroutine. The first trial Mach disc is dropped when the triple-point solution yields a Mach disc slipstream angle less than 15°. This occurred at X = 2.88. The trial Mach disc location of X/r_j = 3.35 produced an acceleration to a Mach number of .7. Profiles at this location, upstream and downstream of the Mach disc, are given in Fig. 7D and E. The pressure ratios across the Mach disc and barrel shock are, respectively, 13 and 5 with the triple-point pressure balance achieved by a reflected shock with a pressure ratio of 2.6. The initial Mach disc slipstream angle at this station was about 10°.

The logistics involved in the automated Mach disc procedure can be gleaned from the variations in slipstream angle, Mach number and streamtube size portrayed in Fig. 8 for various trial Mach disc locations. The first trial location (X_{MD} = 2.88) is well upstream of the correct location as detected by the rapid divergence of the Mach disc streamtube. This type of solution is terminated when either the slipstream angle exceeds 35° or the Mach number in the streamtube falls below .08, as discussed in the previous subsection. The two trial locations of X_{MD} = 3.23 and 3.29 represent positions

one and two integration steps upstream of the trial location yielding acceleration to M = .7. The solutions corresponding to these locations both undergo subsonic to subsonic transitions. The trial solution of X_{md} = 3.35 accelerates to a Mach number of 0.7, but represents a choked branch since the slipstream did not inflect prior to reaching this location.

Referring to Fig. 9, if one imposed a linear M/θ relation (analogous to the P/θ procedure of Ref. 22) downstream of the M = .7 point on the choked branch, the throat size would be underestimated by about 20%. Alternatively, if one imposed this linear relation starting from the inflection point on the previous subsonic/subsonic branch, the throat size would be overestimated by more than 10%. Neither of these procedures appears particularly appealing. In view of the large negative angle at the M = .7 point on the choked solution branch, the parabolic fit procedure linked to this point would also yield a nonrealistic solution curve. This case represents one in which the correct solution lies between the subsonic/subsonic and choked branches and for which neither of these branches can be "forced" through a throat without producing substantial errors in the solution. For this case, the last subsonic/subsonic solution is employed with the triple-point solution perturbed as discussed in Section 3.5.4. The perturbed integral curve (obtained by decreasing θ_{MD} at X_{MD} = 3.29) is seen to nearly bisect the choked and subsonic/subsonic integral curves. Downstream of the M = .7 point, the quadratic relation given by Equation (27) is shown to smoothly accelerate the solution through a sonic throat.

The second test case presented exhibits multiple inviscid cell capabilities for a situation with negligibly small Mach disc sizes. The case is that of a slightly overexpanded (P_j/P_∞ = .874) M = 2.4 jet exhausting from a conical nozzle (10° lip angle) into still air. The calculation was performed with 81 radial grid points (to resolve the shock strengthening in the vicinity of the axis) and employed a perfect gas option (γ = 1.33). The axial pressure distribution for the first seven inviscid cells (and flowfield schematic for the first three cells) is depicted in Figure 10. The flow pattern exhibits strong nonlinearities in the first three inviscid cells and achieves a linearized, repetitive pattern downstream of the third cell.

4. OVERLAID ANALYSIS OF TURBULENT MIXING AND AFTERBURNING PROCESSES

4.1 Methodology

Turbulent mixing processes in the shear layer growing along the plume interface (Fig. 1) are analyzed by BOATAC, for nonafterburning plumes, and by BOATAB, for afterburning plumes. The mixing calculation is initiated at the nozzle exit plane (or at the reattachment point if separation occurs) and "overlaid" on a flowfield map comprised of inviscid solutions of the supersonic plume exhaust and external subsonic/transonic flow (Fig. 11). In the overlaid procedure, the parabolic mixing layer equations are solved subject to variable edge conditions and pressure gradients, determined in accordance

with the growth of the mixing layer and the prescribed inviscid flowfield maps. The details of the overlaid procedure are available in Refs. 6, 8, 9; however, the procedure for determining the rate of computational boundary growth is new and is described below.

The parabolic equations employed in the mixing analysis have been revised from the original formulation so that total enthalpy replaces temperature as the dependent variable in the energy equation. In addition, cubic polynomials are used in the property resetting procedure improving upon the accuracy of the original code. Both new versions of BOAT have self-contained thermodynamic packages. BOATAB has, in addition, a self-contained chemical-kinetic package for aircraft exhausts, and retains the same efficient implicit procedure for treating the chemical source term in the integration of the species continuity equation (see Ref. 6).

The overall computational procedure remains unchanged from that detailed in Ref. 6 with an equal number of grid intervals spanning the shear layer *and* the integration performed along the "actual" streamlines. Both new BOAT codes retain the extended mixing-length and kε2, two-equation turbulence models employed in the original formulation.

4.2 Governing Equations

Mixing processes in the shear layer growing along the plume interface are adequately described by the standard parabolic jet mixing equations provided the plume interface angles are relatively small. (For plumes with a significant degree of underexpansion, a plume-oriented boundary layer coordinate system (see Ref. 23) would be required.) The jet mixing equations, cast in transformed (x, ψ) coordinates are listed below.*

$$\boxed{\frac{\partial f}{\partial x} = \frac{1}{\psi} \frac{\partial}{\partial \psi} \left(\frac{A}{\sigma} \frac{\partial f}{\partial \psi} \right) + g} \tag{31}$$

where

$$f = \begin{pmatrix} u \\ H \\ F_i \\ k \\ \varepsilon \end{pmatrix}; \quad \sigma^{-1} = \begin{pmatrix} 1 \\ Pr^{-1} \\ Pr^{-1} \\ 1. \\ .77 \end{pmatrix}$$

*The chemical source term, w_i, appearing in the g vector array is, of course, zero in BOATAC which treats nonafterburning exhaust plumes.

$$g = \begin{pmatrix} -1/\rho u \, \frac{\partial p}{\partial x} \\ \frac{1}{\psi} \, \frac{\partial}{\partial \psi} \left[A(1-1/Pr) u \, \frac{\partial u}{\partial \psi} \right] \\ \dot{w}/\rho u \\ (P-\varepsilon)/u \\ (C_1 P - C_2 \varepsilon)\varepsilon/uk \end{pmatrix}$$

In these equations, u is the axial velocity; H, the total enthalpy; F_i the mole fraction of the i^{th} species divided by the mixture molecular weight, k, the turbulent kinetic energy; and ε, the rate of turbulent dissipation. The term, A, is given by

$$A = \mu_t \, \frac{\rho u r^2}{\psi} \tag{32a}$$

and the turbulence production term, P, by

$$P = \frac{Au}{\psi} \left(\frac{\partial u}{\partial \psi}\right)^2 \tag{32b}$$

In writing equation (31), it has been tacitly assumed that the turbulent Lewis number is unity.

The transformation from cylindrical (x,r) to streamfunction (x,ψ) coordinates is given by

$$\psi \frac{\partial \psi}{\partial r} = \rho u r \tag{33a}$$

$$\psi \frac{\partial \psi}{\partial x} = -\rho v r \tag{33b}$$

The turbulent viscosity, μ_t, in the kε formulation is given by

$$\mu_t = C_\mu \, \frac{\rho k^2}{\varepsilon} \tag{34}$$

where C_μ and the constants C_1 and C_2 employed in the ε equation are described in Ref. 6. In application of the extended mixing length turbulence model, the k and ε equations are not required and μ_t is given by

$$\mu_t = \rho \ell^2 \left|\frac{\partial u}{\partial r}\right| \tag{35}$$

The various expressions employed for the mixing length, ℓ, are given in Ref. 6. A detailed assessment of these (and several other) turbulence models using BOAT to predict a spectrum of free shear layer problems, with and without chemical reactions, has been presented in Ref. 24.

The system of Equations (31) is supplemented by the equation of state

$$P = \frac{\rho RT}{W} \tag{36}$$

where

$$W = 1./ \sum_{i=1}^{NS} F_i$$

and the temperature is determined via inversion of the static enthalpy relation

$$h(T) = \sum_{i=1}^{NS} h_i(T) F_i W = H - \tfrac{1}{2} u^2 \tag{37}$$

with $h_i(T)$ given by the polynomial fits of Equations (8) and (9). In BOATAC, thermodynamic data is contained for the six species, N_2, O_2, CO_2, H_2O, CO and CH_4. In BOATAB, this species list is extended to include data for CH_3, OH, H_2, H, and O. NS in the above summations, denotes the number of species.

4.3 Computational Scheme

At the axial station, x, a fixed number of grid intervals span the computational domain bounded by $\psi_1(x)$ and $\psi_2(x)$ (Fig. 12). In integrating the system of equations (Eq. 31) from x to $x+\Delta x$, the following sequence of operations is involved:

(1) The computational boundary growth rate, ψ_x, is determined explicitly yielding ψ_1 and ψ_2 at $x + \Delta x$.

(2) The properties are reset at x via a cubic interpolation procedure with grid points redistributed over the extended interval $\psi_1(x+\Delta x)$ to $\psi_2(x+\Delta x)$.

(3) Boundary conditions at $x + \Delta x$ are determined from inviscid flowfield maps at the locations corresponding to ψ_1 and ψ_2 (see Ref. 6 for details).

(4) The equations are integrated from x to $x + \Delta x$ along the streamlines, ψ = const., using an explicit procedure for the momentum, energy and turbulence equations and a mixed implicit/explicit procedure for the species continuity equation in situations with finite rate chemistry. The local pressure gradient, $\partial p/\partial x\ (x,\psi)$, is determined from the inviscid maps and the turbulent viscosity is calculated using Equations (34) or (35).

(5) The temperature is determined by an iterative inversion of the static enthalpy fit; auxiliary variables, W and ρ are then determined, with the pressure distribution $p\ (x,\psi)$ extracted from the inviscid maps.

(6) The radial location of the grid points, $r(x,\psi)$, is determined by inversion of Equation (33a) while the normal velocity component, $v\ (x,\psi)$, is determined from Equation (33b).

(7) The "effective" plume boundary shape is calculated employing a displacement thickness correction obtained by an axial integration of the asymptotic normal velocity, $v_e(x) = v(x,\psi_2)$.

The sequence of calculations (1) - (7) is started by specification of initial profiles across the mixing layer at the nozzle exit plane. Details of the above operations will be given below.

4.4 Computational Boundary Growth

In the original formulation of BOAT,[6] the growth rates of the computational boundaries, $\psi_1(x)$ and $\psi_2(x)$, were given by "rules" akin to those originally suggested by Patankar and Spalding.[25] Different rules were employed for different turbulence models which had to be supplemented by additional tests on edge gradients to prevent the build up of either edge gradients or large tails. The requirement for incorporating additional edge tests sug-

gested that the use of these supposedly general growth rules was, in fact, superfluous.

The new approach taken requires no growth rules. It works by continuously monitoring the edge gradients and altering the local growth rates to keep edge gradients within prescribed bounds. The process is initiated by stipulating values for ψ_{x_1} and ψ_{x_2}; any reasonable estimates will suffice. For an initial shear layer, the expressions

$$\psi_{x_{1,2}} = \frac{(\rho u)_{1,2}{}^{r}}{2\psi\ \sigma_o} \left| \frac{1-u_1/u_2}{1+u_1/u_2} \right| \tag{38}$$

are employed where u_1/u_2 is the velocity ratio and σ_o is the incompressible shear layer spread rate parameter with one stream stationary ($\sigma_o \sim 10$). The initial integration step is taken with these values of $\psi_{x_{1,2}}$. At each subsequent integration step, the nondimensional edge gradients (the * values are one grid point in from the edges)

$$\overline{u}_{1,2} = \left| \frac{u^* - u_{1,2}}{u_1 - u_2} \right| \tag{39a}$$

and

$$\overline{H}_{1,2} = \left| \frac{H^* - H_{1,2}}{H_1 - H_2} \right| \tag{39b}$$

are constructed and the following logical tests are performed.

(a) The values of $\psi_{x_{1,2}}$ are *not* altered if:

(1) both $\overline{u}_{1,2}$ and $\overline{H}_{1,2}$ are between .01 and .02.

(2) either $\overline{u}_{1,2}$ or $\overline{H}_{1,2}$ is less than .01 and the other variable is between .01 and .02.

(b) The values of $\psi_{x_{1,2}}$ are doubled if either $\overline{u}_{1,2}$ or $\overline{H}_{1,2}$ are greater than .02.

(c) The values of $\psi_{x_{1,2}}$ are halved if both $\bar{u}_{1,2}$ and $\bar{H}_{1,2}$ are less than .01.

The factors used to increase/decrease $\psi_{x_{1,2}}$ (presently 2 and $\frac{1}{2}$) and the tolerance limits of .01 to .02 appear to work adequately. Optimal values of these constants/limits have not yet been established.

4.5 Redistribution of Grid Points

Prior to performing the integration from x to x + Δx, the grid points at x are redistributed to span the extended computational domain $\psi_1(x + \Delta x) < \psi < \psi_2 (x + \Delta x)$

where

$$\psi_{1,2} (x + \Delta x) = \psi_{1,2}(x) + \psi_{x_{1,2}} \Delta x \tag{40}$$

The number of equally spaced grid intervals employed (MPSI-1) remains constant throughout the course of the calculation. With the grid spacing, $\Delta\psi(x)$, defined by

$$\Delta\psi(x) = \frac{\psi_2(x) - \psi_1(x)}{\text{MPSI-1}} \tag{41}$$

the grid points, k, at station x, having streamfunction values

$$\psi_k = \psi_1(x) + (k-1)\ \Delta\psi(x) \tag{42}$$

are repositioned at the streamfunction values

$$\tilde{\psi}_I = \psi_1(x+\Delta x) + (I-1)\Delta\psi(x+\Delta x) \tag{43}$$

The values of the dependent variables, $\tilde{f}$, of Equation (31) (at x) are

determined at the locations, $\tilde{\psi}_I$, by the cubic interpolation*

$$\tilde{f}_I = a + br + cr^2 + dr^3 \tag{44}$$

where

$$a = f_{k-1}$$

$$b = .5(f_k - f_{k-2})$$

$$c = -.5f_{k+1} + 2f_k - 2.5f_{k-1} + f_{k-2}$$

$$d = .5f_{k+1} - 1.5f_k + 1.5f_{k-1} - .5f_{k-2}$$

and

$$r = (\tilde{\psi}_I - \psi_{k-1})/\Delta\psi(x)$$

with

$$\psi_{k-1} \leq \tilde{\psi}_I \leq \psi_k$$

4.6 Temperature Inversion

With the satisfactory completion of an integration step, the temperature is determined from the mixture static enthalpy and species concentration. The required temperature inversion is performed once per grid point at each integration step, and, is done after the interpolative procedure of Section 4.5. A self convergent procedure is employed initiated by the previous temperature at the grid point of interest; viz., $T^{(i)} = T^{(i-1)} - (h^{(i-1)}-h^*)/C_p^{(i-1)}$ where i designates the iteration counter, h* is the

*The interpolating cubic duplicates the function and its first derivative (evaluated by a central difference formula) at the points k and k-1.

stipulated value of static enthalpy, $h^{(i-1)} = h(T^{(i-1)}, F_j)$, and $C_p^{(i-1)} = C_p(T^{(i-1)}, F_j)$, as given by the polynomial curve fits. Convergence is generally obtained in three iterations even in regions of rapid change.

4.7 Integration Procedure

The system of equations (Eqs. 31) in non-afterburning exhausts is integrated from x to x + Δx by a one step, explicit procedure, along the streamlines, $\tilde{\psi}_I$. The finite-difference formulation is given by

$$f_I(x+\Delta x) = f_I(x) + \frac{\Delta x}{\sigma\psi_I}\frac{\partial}{\partial\psi}\left(A(x)\frac{\partial f}{\partial\psi}\right)_I + g(x)_I\Delta x \qquad (45)$$

where

$$\frac{\partial}{\partial\psi}\left(A\frac{\partial f}{\partial\psi}\right)_I = \frac{A(x)_{I+1}+A(x)_I}{2(\Delta\psi)^2}\left(f(x)_{I+1} - f(x)_I\right)$$

$$- \frac{A(x)_{I-1}+A(x)_I}{2(\Delta\psi)^2}\left(f(x)_I - f(x)_{I-1}\right)$$

and first derivative expressions appearing in $g(x)_I$ are given by

$$\frac{\partial f}{\partial\psi} = \frac{f(x)_{I+1}-f(x)_{I-1}}{2\Delta\psi}$$

4.8 Treatment of Finite Rate Chemistry

The treatment of afterburning in the mixing layer associated with exhausts containing unburnt fuel is provided for in the BOATAB code. BOATAB is formally identical to BOATAC with the addition of chemical kinetic capabilities. The reaction mechanism and rate coefficients* incorporated in BOATAB are listed below:

*The rate coefficient is defined as $k_f = AT^{-N}\exp(E/RT)$.

Reaction		A	N	E
(1) $H + OH + M$	$= H_2O + M$	1.E-25	2.0	0.
(2) $O + H + M$	$= OH + M$	3.E-32	0.	0.
(3) $O + O + M$	$= O_2 + M$	5.E-30	1.	-340.
(4) $H + H + M$	$= H_2 + M$	5.E-30	1.	0.
(5) $CO + O + M$	$= CO_2 + M$	1.E-32	0.	-4000.
(6) $OH + H$	$= H_2 + O$	1.4E-14	-1.	-7000.
(7) $OH + O$	$= H + O_2$	4.E-11	0.	0.
(8) $OH + H_2$	$= H_2O + H$	1.E-17	-2.	-2900.
(9) $OH + OH$	$= H_2O + O$	1.E-11	0.	-1100.
(10) $OH + CO$	$= CO_2 + H$	1.1E-19	-2.	1600.
(11) $CH_4 + OH$	$= CH_3 + H_2O$	5.E-11	0.	-5000.
(12) $CH_3 + O_2$	$= CO + OH + H_2$	5.E-10	0.	-5000.

The reaction mechanism comprises what has become a standard set of chemical reactions for the combustion of CO and H_2 (reactions 1 to 10) in rocket exhaust plumes,[26] plus, a two-step global oxidation mechanism for CH_4. The latter is made up of the predominant rate-controlling initial attack step in CH_4 flames, [27] followed by a rapid conversion of the resultant CH_3 intermediate to CO and H_2. A detailed study establishing the validity of this two-step global mechanism has not been performed. Modifications to the program to include additional reactions (up to 40) and/or species (up to 25) involves a simple extension of present data blocks.

The implicit treatment and linearization of the chemical source term in the species continuity equation is described in Ref. 6. Via this implicit treatment, no "formal" stability limitation on the integration step is imposed by the chemistry. The basic marching step is then limited by standard parabolic stability considerations associated with the explicit formulation (see Ref. 6). However, in regions of rapid chemistry, a control on the allowable temperature change per integration step is used to insure accuracy. In the original BOAT formulation, the step size employed in this controlling process was arrived at by successive halving of the standard step size. This proved to be quite inefficient since the halving process was performed at each integration step starting from the stability dictated parabolic step-size (i.e., no cognizance was taken of the step-size reduction required in the previous integration step). Included in BOATAB is a new approach for controlling the step-size in regions of rapid chemistry, developed under the JANNAF Rocket Plume Standardization effort. Applications of this new chemistry step-size control have decreased overall run times

by more than a factor of 2 for rocket plume calculations involving rapid chemistry. A brief description of this new approach is as follows:

(1) The maximum permissible temperature change in an integration step, TCONT, is specified.

(2) Control factors FDL and DFDL are initialized with values of 1.

(3) The equations are integrated employing the integration step

$$\Delta X = FDL * \Delta X_{par}$$

where ΔX_{par} is the step size dictated by stability requirements.

(4) The temperature change, ΔT, is determined along the streamline whose value of temperature is maximum.

(5) The following test is performed:

If $(\Delta T/TCONT) \geq 1$, FDL = FDL/2 and Steps (3) - (5) are repeated.

If $(\Delta T/TCONT) \leq 1$, the integration is complete and FDL is not changed.

(6) DFDL is determined by the relation

DFDL = INT (TCONT/ΔT)

(where INT denotes an integerizing process) and FDL for the next integration step is given by

FDL = FDL * DFDL

subject to the constraint that FDL < 1.

This procedure determines the maximum permissible integration step that yields temperature changes less than that prescribed. The step is monitored continuously and is increased when the chemistry slows down and decreased when the chemistry speeds up. Decreases always occur via halving FDL from the value that "worked" in the previous integration step. Increases are abrupt with a rapid adjustment provided by the DFDL factor. For example, when first entering a region of rapid chemistry, several step-size reductions may be necessary to arrive at the appropriate FDL factor. In the next few steps, FDL may require some further halving until an appropriate level is established. This value of FDL will then generally suffice throughout the region of rapid chemistry (subject to possible small modifications associated

with wave effects -- i.e., chemistry speeding up in regions of compression and slowing down in expansive regions). As the chemistry slows down, DFDL serves to boost FDL towards unity until temperature changes due to chemistry no longer control the integration step.

4.9 Initialization Options

The user has the option of stipulating an initial profile or using built in initialization options. The built in options provide for a shear layer profile, a boundary layer profile, or a separated flow profile at the point of reattachment.

In the user specified initialization option, the user inputs the distribution of $u(r)$, $T(r)$ and $\alpha_i(r)$ at an arbitrary x station. If no information is available regarding inital turbulence levels, the turbulent viscosity will be determined using the extended mixing length (ML) model. Note, however, that for complex distributions containing more than 2 velocity maxima or minima, an extension of the dual length scale procedure presently included will be required (see Ref. 6). In the $k\varepsilon$ option, the distribution of $k(r)$ and $\varepsilon(r)$ is determined from the ML viscosity distribution, $\mu_t(r)$ via the relations (see Ref. 6)

$$k(r) = \frac{\mu_t(r) \mid \partial u/\partial r \mid}{.3\ \rho(r)} \tag{46}$$

and

$$\varepsilon(r) = \frac{.09\rho(r)k^2(r)}{\mu_t(r)} \tag{47}$$

If the $k(r)$ profile is known at the initial station, $\mu_t(r)$ is determined via an inversion of Equation (46) and $\varepsilon(r)$ again from Equation (47).

In the shear layer initialization option, profiles of the form

$$\frac{u-u_1}{u_2-u_1} = \frac{H-H_1}{H_2-H_1} = \frac{F_i-F_{i_1}}{F_{i_2}-F_{i_1}} = 3\eta^2\left(1 - \frac{2}{3}\eta\right) \tag{48}$$

are distributed across the shear layer ($0 \le \eta \le 1$) where $\eta = (r-r_1)/(r_2-r_1)$. The shear layer width, r_2-r_1, is estimated by

$$r_2 - r_1 = .27 \frac{(u_1 - u_2)}{(u_1 + u_2)} x \tag{49}$$

and centered about the plume interface, $r_c(x)$ at the initial station x. Properties at 1 and 2 are determined from the inviscid maps.

In the boundary layer initialization option, velocity profiles of the form[12]

$$\frac{u(r)}{u_{1,2}} = \left(\frac{\eta}{\delta_{1,2}}\right)^{1/n_{1,2}} \tag{50}$$

are employed where $\eta = | r - r_c |$ and the boundary layer thicknesses, $\delta_{1,2}$, and exponents, $n_{1,2}$ are specified. Temperature profiles are determined assuming $H_{1,2}$ to be constant:

$$\frac{T(r)}{T_{1,2}} = 1 + \frac{(\gamma_{1,2} - 1)}{2} M^2_{1,2} \left[1 - \left(\frac{u(r)}{u_{1,2}}\right)^2\right] \tag{51}$$

In the separated flow initialization option, a reattachment velocity profile of the form[13]

$$\frac{u}{u_{1,2}} = 2 \left(\frac{\eta}{\delta_{1,2}}\right)^{3/2} - \left(\frac{\eta}{\delta_{1,2}}\right)^3 \tag{52}$$

is employed where the thickness $\delta_{1,2}$ are specified. The temperature profiles are determined employing Equation (51).

4.10 Effective Plume Geometry

In the performance of an overlaid BOAT calculation, the asymptotic normal velocity variation, $v_e(x) = v(\psi_2(x))$, is determined via inversion of Equation (33b). This velocity variation is used to determine the "effective" plume boundary, $r_{eff}(x)$, displaced from the inviscid plume interface $r_c(x)$, by the mixing induced displacement thickness, $\delta^*(x)$. This displacement is generally called the jet entrainment effect.

A mass balance from the jet axis to r_e, the outer shear layer boundary (see Fig. 11) yields

$$\rho_e U_e \left[(\delta^* + r_c)^2 - r_c^2\right] = \int_o^{r_c} \rho_J U_J dr^2 + \int_{r_c}^{r_e} \rho_e U_e dr^2 - \int_o^{r_e} \rho u dr^2 \qquad (53)$$

where $u(r,x) = U_j(r,x)$ for $r = 0$ to r_1. Taking d/dx of Equation (53) (noting that the 1st r.h.s. integral is a constant proportional to the mass flux in the inviscid exhaust and assuming the radial variation of $\rho_e U_e$ to be negligible) yields

$$\rho_e U_e \frac{dr^2}{dx}_{eff} + r_{eff}^2 \frac{d}{dx}(\rho_e U_e) = \frac{d}{dx}(\rho_e U_e r_e^2) - 2\rho_e U_e r_e \frac{dr_e}{dx} - \frac{d}{dx}(\psi_e^2)$$

where $r_{eff} = r_c + \delta^*$ and the third integral on the r.h.s. of Equation (53) has been transformed employing Equation (33a). Making use of Equation (33b), one obtains the following differential equation for $r_{eff}(x)$:

$$\frac{d}{dx} r_{eff}^2 + (r_{eff}^2 - r_e^2) \frac{d\ln \rho_e U_e}{dx} = 2 r_e \frac{v_e}{U_e} \qquad (54)$$

The boundary comprised of the nozzle afterbody displaced by the boundary layer displacement thickness, and, the effective plume geometry, $r_{eff}(x)$, is employed to determine the external flow pressure field. The iterative sequence involved in revising the inviscid plume shape (using SCIPAC) and revising the entrainment effect (using BOATAC or AB overlaid on the SCIPAC and external inviscid flow maps) is detailed in Refs. 1 and 2.

4.11 Calculations

Versions of the BOAT codes have been employed to perform a broad spectrum of calculations for plume related flowfields. A summary of constant pressure, free mixing calculations performed is provided in Table I. Applications of the BOAT code in the overlaid mode, in the patched NASA/LRC system, have been reported in Refs. 1, 2, 6, 8, and 9. These calculations present system results for cold air jets at various pressure ratios for external Mach numbers of 0.4 and 0.8, and, additional calculations for hot jets with and without afterburning. Overlaid calculations for afterburning rocket plumes (employing BOAT and SCIPPY) have been reported in Refs. 28 and

29. The present versions of BOAT (BOATAC and AB) will provide comparable results to those reported in a substantially more efficient manner by virtue of the modifications reported herein.

5. CODE/SUBROUTINE DESCRIPTIONS

5.1 SCIPAC

A subroutine flow chart for SCIPAC is depicted in Fig. 13. The main driver is PY and the overall code is divided into two sections; an initialization section controlled by IN and an integration section controlled by CT. The user specifies nozzle exit conditions, the pressure distribution along the plume interface and file names. SCIPAC performs the underexpansion interaction at the lip and fills the vector arrays E, F, and G at IMAX grid points evenly spaced between the axis and plume interface, after stepping out a small axial distance from the exit plane to provide some grid definition of the flow in the lip region. The user has the choice of selecting a perfect or real gas option and an Abbett or Sting Mach disc procedure.

In the integration loop, the marching step is determined and a predictor/corrector procedure is employed solving the lower and upper boundary points first, and then, all interior points. After the sequence of operations, at both the predictor and corrector levels, the conservation variables are decoded and new F and G vector arrays are constructed. This basic procedure is supplemented by routines which analyze the flow in the Mach disc and perform the triple-point calculations. A description of the functions performed by the various subroutines in SCIPAC is provided below:

BL: Performs the lower boundary point calculation employing the limiting form of the conservation equations (Equation 4) at an axis or characteristic procedures (Equations 19-24) along the Mach disc slipstream or solid sting. The logical decisions associated with the Mach disc calculation are performed in this routine.

BU: Performs the upper boundary point calculations via characteristic procedures (Equations 19-24) in conjunction with a specification of the pressure distribution along the plume interface via a call to EX.

CE: For conical exhausts, CE determines properties in the plume core (between the axis and leading downrunning characteristics from the nozzle lip), and is used only in the initialization procedure.

CF: Contains the thermodynamic data for the six species N_2, O_2, CO_2, H_2O, CO, and CH_4. Calculates the mixture polynomial coefficients of Equation (10), the low temperature coefficients of Equation (9), and the mixture molecular weight

CT: Provides overall control of the integration portion of SCIPAC (see the flow chart).

DC: Decodes the conservation variables as described by Equations (15-18).

DK: Performs an isentropic expansion/compression to ambient pressure on an individual streamline basis over a prescribed length scale starting from the axial station X = XDK (Section 3.5.7).

DX: Determines the maximum allowable marching step, DX, satisfying the CFL criterion at all grid points. Formal characteristic intersections are employed.

EE: Determines the vector array, E, of Equation (1).

ER: Iterative routines used to determine pressure/flow deflection balance across Mach disc slipstream.

EX: Provides pressure along plume interface.

FG: Determines the vectors arrays, F and G of Equation (1).

GM*: Determines the specific heat ratio, γ, via Equations (12) and (13).

HS*: Determines the static enthalpy via Equation (11).

IN: Reads in the required input data and controls the overall flowfield initialization (see the flow chart).

IP: Performs the interior point integration via Equations (14a) and (14b).

MD: Integrates the 1-D equations in the Mach disc streamtube (Equations 29a, b, and c).

OT: Output routine.

PM: Determines the initial plume interface angle via a calculation of the lip Prandtl-Meyer expansion so that a pressure balance with the external flow is achieved.

PT: Determines properties for characteristic calculations.

---

*Functions

PY: Main driver routine (see flow chart).

RE: Resets variables at the end of an integration step.

RS: Restart routine.

SH: Shock point calculation routine. Performs the operations entailed in Section 3.5.3.

TP: Triple-point routine. Performs the logical decisions involved at the triple-point which include locating the barrel shock, determining properties behind the Mach disc and reflected shocks, and deciding if the Mach disc should be dropped (see Section 3.5).

A description of input required for SCIPAC is provided in Appendix I.

5.2 BOATAC and BOATAB

The subroutine flow charts for BOATAC and BOATAB are depicted in Figs. 12 and 13. The structure of these codes differs only in the addition of subroutines S2, CC, SL and EF in BOATAB, which comprise the chemistry package. The main driver is MØ and the overall code is divided into two sections; an initialization section controlled by SB and an integration section controlled by M1. The user specifies an initialization option (or profile) and several input parameters in SA which processes this data and the thermodynamic data via a call to SD. The formal initialization procedure is controlled by SB with initial mixing layer profiles generated in IP, turbulence profiles in KE and inviscid map processing performed in IF.

In the integration loop, M1 performs the executive duties and determines the allowable marching step and subsidiary variables. The viscosity distribution is determined in VI, and the pressure variation across the mixing layer from the inviscid data maps in II. In BOATAC, the integration is performed in S3 with edge conditions from the inviscid maps determined from II. In BOATAB, the chemistry processing is performed in S2 and the standard integration in S3. When the integration is complete, M2 checks the temperature change in the integration step. If the change is larger than TCONT, FDL is halved and the integration is repeated (see Section 4.8). When the integration step is completed, the computational boundary growth is computed in EN and the profiles are reset in M2 over the extended domains. The sequential integration of the effective plume boundary differential equation is performed in DS. A more specific description of the tasks performed by the various subroutines in BOATAC and BOATAB is provided below:

CC: Determines the chemical reaction rates (see Ref. 6).

DS: Determines the effective plume geometry via integration of Equation (54).

EF: Calculates the equilibrium constant for determining the backward reaction rates (see Ref. 6).

EN: Calculates the computational boundary growth as described in Section 4.4.

HX: Determines the static enthalpy and specific heat at constant pressure.

IF: Generates mapped vector arrays for the inviscid exhaust and external flows from the inviscid files supplied (see Ref. 6 for details).

II: Extracts information from the mapped vector arrays created in IP.

IN: Output routine for initial variables and run parameters.

IP: Calculates initial shear layer, boundary layer or reattachment point profiles (see Section 4.9).

KE: Performs the initialization for turbulence parameters (see Section 4.9).

LI: Linear interpolation routine.

MØ: Main driver routine (see flow chart).

M1: Controls integration loop. Also determines stepsize and auxiliary variables W, ρ, and r.

M2: Checks temperature change in integration step and performs grid point redistribution via cubic polynomials (see Section 4.5).

OT: Output routine.

SA: Reads in input data.

SB: Controls the initialization loop.

SD: Contains the thermodynamic data for the 6 species in BOATAC and the 11 species in BOATAB. Performs the manipulation of these data.

SL: Performs the matrix inversion required in the solution of the species continuity equations (see Ref. 6).

S2: Controls the finite-rate chemistry integration (see Ref. 6).

S3: Integrates the flowfield equations as discussed in Section 4.7.

TX: Performs the iterative inversion of the temperature from known values of h and F_i.

VI: Calculates the turbulent viscosities employing either the ML or kε formulation (Equations (34) or (35)).

A description of input required for BOATAC and BOATAB is provided in Appendix II.

6. CONCLUDING REMARKS

Computer codes have been described which provide for the viscous/inviscid analysis of jet aircraft exhaust plumes via an overlaid procedure. SCIPAC is an efficient inviscid shock-capturing model with real gas capabilities and a fully-automated treatment of the Mach disc region. Two viscous, turbulent mixing codes, BOATAC and BOATAB, have been described which are optimized versions of the original BOAT code described in Refs. 6 and 7. These codes have been entirely restructured and contain improvements in the integration of the energy equation, the computational boundary growth formulation, the redistribution of grid points, the chemistry step-size procedure and the treatment of thermodynamic properties.

Both SCIPAC and BOATAC/AB are integral components of the NASA/LRC system for predicting nozzle afterbody drag. The description and performance of this system has been reported in Refs. 1 and 2. The formulation of the overlaid procedure and the effective plume boundary concept for predicting the effect of jet entrainment on afterbody drag have been reported in Refs. 6, 8, and 9. Sensitivities of afterbody drag to such parameters as : turbulence model formulation, pressure gradient variations in the mixing layer and initial conditions have been reported in Refs. 6, 8, and 9. An extension of such studies has been reported in Refs. 1 and 2.

APPENDIX I
INPUT INSTRUCTIONS FOR SCIPAC

Column	Fortran Name	
		Card 1
1-8 (8A1)	FILENM	First Mach disc scratch file
9-16 (8A1)	FILENN	2nd Mach disc scratch file
		Card 2
1-5 (I5)	IREAD	Number of input data points (use 2 for uniform or conical flow)
6-10 (I5)	IMAX	Number of grid points for run (max. of 81)
11-15 (I5)	IFLOW	= 1 for cylindrical coordinates
16-20 (I5)	ICHEM	= 0 for perfect gas = 1 for real gas
21-25 (I5)	IBL	Lower boundary indicator = -1 for axis or plane of symmetry
26-30 (I5)	IBU	Upper boundary indicator = 1 for specified pressure
31-35 (I5)	IEXT	Number of pressure data stations. For constant pressure external boundary, set IEXT = 0.
36-40 (I5)	INT	Number of grid intervals in barrel shock layer initialization. For low pressure ratios, set INT = 0.
		Card 3
1-16 (2A8)	BTFILE	Name of file supplied to BOAT code for overlaid mixing calculation (leave blank if no file is to be created).
		Card 4
1-10 (E10.0)	XSTART	Starting value of XM (units arbitrary, RJ converts to feet)

Column	Fortran Name	Card 4 (Continued)
11-20 (E10.0)	XSTOP	Final value of XM (units arbitrary)
12-30 (E10.0)	DXPRNT	Initial print interval (units arbitrary)
31-40 (E10.0)	XCHNG	XM for change in print interval (units arbitrary)
41-50 (E10.0)	XPRNEW	Next print interval (units arbitrary)
51-60 (E10.0)	RX	Step size multiplier (set = 1, unless step size reduction required initially)
61-70 (E10.0)	DRX	At each step, RX = RX + DRX until RX = .9
71-80 (E10.0)	XDK	XM station at which SCIPDK is called (units arbitrary)
		Card 5
1-10 (E10.0)	WMIX	Mixture molecular weight (not needed if ICHEM = 1)
11-20 (E10.0)	GAMJ	Mixture specific heat ratio (not needed if ICHEM = 1)
21-30 (E10.0)	PINF	Ambient pressure (atm)
31-40 (E10.0)	RJ	Scaling parameter. Values of XM and XN output on BTFILE are multiplied by RJ to convert them to feet.
41-50 (E10.0)	XMD	Mach disc parameter = -1 for sting option = 0 for Abbett option with first Mach disc location selected internally = XM for Abbett option initiated by first guess for Mach disc location at XM
51-60 (E10.0	EMXILN	Mach number at which parabola is inserted (see Sect. 3.5.4); set = .7

*The next card is required only if ICHEM = 1.

Column	Fortran Name	Card 6*
1-10 (E10.0)	ALP(1)	Mole fraction N_2
11-20 (E10.0)	ALP(2)	Mole fraction O_2
21-30 (E10.0)	ALP(3)	Mole fraction CO_2
31-40 (E10.0)	ALP(4)	Mole fraction H_2O
41-50 (E10.0)	ALP(5)	Mole fraction CO
51-60 (E10.0)	ALP(6)	Mole fraction CH_4

Card 7.1

1-10 (E10.0)	XN(1)	XN of 1st grid point (units arbitrary, RJ converts to feet)
11-20 (E10.0)	U(1)	Velocity component in XM direction (ft/sec) at 1st point
21-30 (E10.0)	V(1)	Velocity component in XN direction (ft/sec) at 1st point
31-40 (E10.0)	P(1)	Pressure (atm) at 1st point
41-50 (E10.0)	T(1)	Temperature (°K) at 1st point

On cards 8.2, 8.3 - 8.IREAD, repeat above for 2nd, 3rd, --, IREAD grid points.

Prescribed Pressure Data: **The next set of cards is required only if IBU = 1 and the pressure along the plume interface is variable.

Card 8.1**

1-10 (E10.0)	XEXT(1)	XM at 1st pressure data station
11-20 (E10.0)	PEXT(1)	Pressure (atm) at 1st pressure data station

On cards 9.2, 9.3 - 9.IEXT, repeat above for 2nd, 3rd, -- IEXT station.

APPENDIX II
INPUT INSTRUCTIONS FOR BOATAC/AB

Column	Fortran Name	Card 1
1-72	TITLE(I)	Job Identification
		Card 2
1-5 (I5)	MPSI	Number of radial data points in user specified initial profile (IDELP = 1), number of points for run in other initialization options (maximum of 50)
6-10 (I5)	NMPSI	Number of points for run if initial profile is user specified (maximum of 50), for other options set NMPSI = MPSI
11-15 (I5)	IDELP	Indicator for specifying initial radial profiles = 0, shear layer profile calculated internally = 1, user specified profile = -1, boundary layer profiles calculated internally = -2, reattachment profiles calculated internally
16-20 (I5)	IPRESS	Inviscid structure indicator = 0, constant pressure mixing = 1, jet map file is read* = 2, jet and external map files are read
21-25 (I5)	IVIS	Viscosity model indicator = 0, Prandtl mixing length model = -1, kεl two equation turbulence model = -2, kε2 two equation turbulence model
26-30 (I5)	IMAXJ	Number of axial stations input for jet exhaust inviscid data map (maximum of 50)

Column	Fortran Name	Card 2 (Continued)
31-35 (I5)	KMAXJ	Number of mapped radial stations desired in jet map (maximum of 25)
36-40 (I5)	IMAXE	Number of axial stations input for external flow inviscid data map (maximum of 50)
41-45 (I5)	KMAXE	Number of mapped radial stations desired in external flow map (maximum of 25)
46-50 (I5)	IMTAU	Turbulence initialization indicator = 0, k profile calculated internally = 1, k profile input

*If only jet map file is read, external flow map properties are determined by isentropic expansion to local plume interface pressure and are assumed uniform in the radial direction.

Card 3

1-8 (A8)	FILE.DAT	Name of jet file generated by SCIPPY (if IPRESS = 0, leave blank)
11-20 (E10.3)	UEDGE	Velocity of external stream (needed if IPRESS = 1)
21-30 (E10.3)	TEDGE	Temperature of external stream (needed if IPRESS = 1)

Card 4

1-10 (E10.3)	X	Initial axial station (ft) (cannot be 0 for IDELP = 0)
11-20 (E10.3)	RJ	Nozzle exit radius (ft)
21-30 (E10.3)	XMAX	Total length of run (ft)
31-40 (E10.3)	PRNT	Print interval (ft)
41-50 (E10.3)	XCHANG	Change printer interval at this axial location (ft)
51-60 (E10.3)	PRNTXC	New print interval (ft)

Column	Fortran Name	Card 4 (Continued)
61-70 (E10.3)	FDL	Multiplies program calculated step size, Δx, in order to reduce step size. Useful in initial regions with steep gradients (e.g., initial boundary layers), typical value for initial boundary layers, FDL = 0.2, to suppress oscillations. For smooth initial profiles set FDL = 1.0.
		Card 5
1-10 (E10.3)	XLE	Turbulent Lewis number (must set = 1.)
11-20 (E10.3)	SIGMA	Turbulent Prandtl number
21-30 (E10.3)	TCONT	Maximum allowable temperature change permitted in an integration step (°K), typically, $5° \leq$ TCONT $\leq 10°$K (default = 400°/NMPSI)
31-40 (E10.3)	TKINET	Chemical kinetics cut-off temperature - chemistry assumed frozen below this value. (If TKINET = 0, the default value of 400°K will be used)
		Card 6
1-10 (E10.3)	P	Ambient pressure (atm)
11-20 (E10.3)	U(1)	Jet velocity (ft/sec) (only required if IPRESS = 0)
21-30 (E10.3)	U(MPSI)	External flow velocity (ft/sec)(only required if IPRESS = 0)
31-40 (E10.3)	T(1)	Jet exhaust temperature (°K) (only required if IPRESS = 0)
41-50 (E10.3)	T(MPSI)	External stream temperature (°K) (only required if IPRESS = 0)
		Card 7
1-10 (E10.3)	FFF	Ratio of ℓ/δ in Prandtl mixing length model in nearfield shear layer region, use FF = .065, must also be input for $k\varepsilon$ models initialization procedure

Column	Fortran Name	Card 7 (Continued)
11-20 (E10.3)	GGG	Ratio of ℓ/δ in mixing length model in fully developed region, use GGG = .08
21-30 (E10.3)	PSID	Input PSID = 1.0 if "effective" plume boundary is to be calculated. Can only be used if IPRESS = 2, PSID *must* be set = 0 if IPRESS = 0
31-40 (E10.3)	DELJ	Jet side boundary layer thickness*
41-50 (E10.3)	DELE	External side boundary layer thickness*
51-60 (E10.3)	USTJ	Exponent in jet side boundary layer profile*
61-70 (E10.3)	USTE	Exponent in external side boundary layer profile*

*If IDELP = -1 (Standard BL option)

$U/U_{edge} = (y/\delta)^{1/n}$ where δ = DELJ or DELE and n = 1/USTJ or 1/USTE

If IDELP = -2 (reattachment profile option)

$U/U_{edge} = 2(y/\delta)^{3/2} - (y/\delta)^3$ where δ = DELJ or DELE

**Cards 8 and 9 are required only if IDELP $\leq$ 0 (i.e., they are not required for a user specified profile).

Card 8**

1-10 (E10.3)	ALPHA(1,1)	Mole fraction of N_2 on jet side
11-20 (E10.3)	ALPHA(2,1)	Mole fraction of O_2 on jet side
21-30 (E10.3)	ALPHA(3,1)	Mole fraction of CO_2 on jet side
31-40 (E10.3)	ALPHA(4,1)	Mole fraction of H_2O on jet side
41-50 (E10.3)	ALPHA(5,1)	Mole fraction of CO on jet side
51-60 (E10.3)	ALPHA(6,1)	Mole fraction of CH_4 on jet side

Column	Fortran Name	Card 8 (Continued)
For BOATAB only, continue as follows:		
61-70 (E10.3)	ALPHA(7,1)	Mole fraction of CH_3 on jet side
71-80 (E10.3)	ALPHA(8,1)	Mole fraction of OH on jet side
		Card 8.1
1-10 (E10.3)	ALPHA(9,1)	Mole fraction of H_2 on jet side
21-30 (E10.3)	ALPHA(10,1)	Mole fraction of H on jet side
31-40 (E10.3)	ALPHA(11,1)	Mole fraction of O on jet side
		Card 9**
1-10 (E10.3)	ALPHA(1,MPSI)	Mole fraction of N_2 on ext. side
11-20 (E10.3)	ALPHA(2,MPSI)	Mole fraction of O_2 on ext. side
21-30 (E10.3)	ALPHA(3,MPSI)	Mole fraction of CO_2 on ext. side
31-40 (E10.3)	ALPHA(4,MPSI)	Mole fraction of H_2O on ext. side
41-50 (E10.3)	ALPHA(5,MPSI)	Mole fraction of CO on ext. side
51-60 (E10.3)	ALPHA(6,MPSI)	Mole fraction of CH_4 on ext. side
For BOATAB only, continue as follows:		
61-70 (E10.3)	ALPHA(7,MPSI)	Mole fraction of CH_3 on ext. side
71-80 (E10.3)	ALPHA(8,MPSI)	Mole fraction of OH on ext. side

Column	Fortran Name	Card 9.1
1-10 (E10.3)	ALPHA(9,MPSI)	Mole fraction of H_2 on ext. side
11-20 (E10.3)	ALPHA(10,MPSI)	Mole fraction of H on ext. side
21-30 (E10.3)	ALPHA(11,MPSI)	Mole fraction of 0 on ext. side

***Cards 10-14 are required only if IDELP = 1 (i.e., for user specified initial profiles).

		Card 10***
1-10 (E10.3)	RIN(1)	Nondimensional radial location (r/RJ) of first grid point out of MPSI user specified points. This point can be the lower edge of a shear layer. Do not input RIN(1) = 0 for axis, start with RIN(1) = .01
11-20 (E10.3)	RIN(2)	Radial location of 2nd grid point, etc. Continue with a total of eight values per card
		Card 11***
1-10 (E10.3)	T(1)	Temperature of first grid point (K)
11-20 (E10.3)	T(2)	Temperature of 2nd grid point (K), etc., eight values per card
		Card 12***
1-10 (E10.3)	U(1)	Velocity at first grid point (ft/sec)
11-20 (E10.3)	U(2)	Velocity at 2nd grid point (ft/sec), etc., eight values per card

***Card 13 is required only when IVIS < 0 and IMTAU = 1 (i.e., when a TKE option is selected with a user specified initial turbulent kinetic energy profile)

Column	Fortran Name	Card 13***
1-10 (E10.3)	XK(1)	Turbulent kinetic energy at first grid point (ft^2/sec^2)
11-20 (E10.3)	XK(2)	Turbulent kinetic energy at 2nd grid point (ft^2/sec^2), etc., eight values per card
		Card 14***
1-10 (E10.3)	ALPHA(1,1)	Mole fraction of N_2 at first grid point
⋮	⋮	⋮
51-60 (E10.3)	ALPHA(6,1)	Mole fraction of CH_4 at first grid point

(Continue for species 7-11 as per Card 8 in running BOATAB).

		Card 14.1
1-10 (E10.3)	ALPHA(1,2)	Mole fraction of N_2 at 2nd grid point
		Continue to Card 14.MPSI in analogous fashion

REFERENCES

1. Wilmoth, R. G.: Viscous-Inviscid Calculations of Jet Entrainment Effects on the Subsonic Flow Over Nozzle Afterbodies, NASA TP-1626, 1980.

2. Wilmoth, R. G.; Dash, S. M.; and Pergament, H. S.: A Numerical Study of Jet Entrainment Effects on the Subsonic Flow Over Nozzle Afterbodies, AIAA Paper 79-0135, New Orleans, LA., Jan., 1979.

3. Dash, S. M.; and Thorpe, R. D.: A New Shock-Capturing/Shock Fitting Computational Model for Analyzing Supersonic Inviscid Flows (The SCIPPY Code), Aeronautical Research Associates of Princeton, Inc., Report No. 366, Nov., 1978.

4. Dash, S. M.: Preliminary Calculations of Supersonic Viscous/Inviscid Interactions Using the Fully-Coupled Version of the SCIPPY Code, Aeronautical Research Associates of Princeton, Inc., Technical Memo. No. 79-3, Feb., 1979.

5. Thorpe, R. D.; Dash, S. M.; and Pergament, H. S.: Inclusion of Gas/Particle Interactions in a Shock Capturing Model for Nozzle and Exhaust Plume Flows, AIAA Paper No. 79-1288, Las Vegas, Nevada, June, 1979.

6. Dash, S. M.; and Pergament, H. S.: A Computational Model for the Prediction of Jet Entrainment in the Vicinity of Nozzle Boattails (The BOAT Code), NASA CR-3075, Dec., 1978.

7. Dash, S. M.; and Pergament, H. S.: The BOAT Code Program Users Manual, NASA CR-159001, Nov., 1978.

8. Dash, S. M.; Wilmoth, R. G.; and Pergament, H. S.: Prediction of Near-field Jet Entrainment by an Interactive Mixing/Afterburning Model, AIAA Paper No. 78-1189, Seattle, WA., July, 1978.

9. Dash, S. M.; Wilmoth, R. G.; and Pergament, H. S.: Overlaid Viscous/Inviscid Model for the Prediction of Near-Field Jet Entrainment, AIAA J., Vol. 17, Sept., 1979, pp. 950-958.

10. Dash, S. M.; Pergament, H. S.; and Thorpe, R. D.: A Modular Approach for the Coupling of Viscous and Inviscid Processes in Exhaust Plume Flows, AIAA Paper 79-0150, New Orleans, LA, Jan., 1979.

11. Dash, S. M.; Pergament, H. S.; and Thorpe, R. D.: The JANNAF Standard Plume Flowfield Model: Modular Approach, Computational Features and Preliminary Results, Proceedings of the JANNAF 11th Plume Technology Meeting, CPIA Pub. 306, Vol. I, 1979, pp. 345-442.

12. Reshotko, E.; and Tucker, M.: Approximate Calculation of the Compressible Turbulent Boundary Layer with Heat Transfer and Arbitrary Pressure Gradient, NASA TN 4154, 1957.

13. Presz, W. M., Jr.; King, R. W.; and Buteau, J. D.: An Improved Analytical Model of the Separation Region on Boattail Nozzles at Subsonic Speeds, NASA CR-3028, July 1978.

14. South, J. D., Jr.; and Jameson, A.: Relaxation Solutions for Inviscid Axisymmetric Transonic Flow Over Blunt or Pointed Bodies, Proceedings of AIAA Computational Fluid Dynamics Conference, July, 1973, pp. 8-17.

15. MacCormack, R. W.: The Effect of Viscosity in Hypervelocity Impact Cratering, AIAA Paper 69-354, 1969.

16. Putnam, E. E.; and Abeyounis, W. K.: Experimental and Theoretical Study of Flowfields Surrounding Boattail Nozzles at Subsonic Speeds, AIAA Paper 76-765, July, 1976.

17. Gordon, S.; and McBride, B. J.: Computer Program for the Calculation of Complex Chemical Equilibrium Compositions, Rocket Performance, Incident and Reflected Shocks, and Chapman-Jouguet Detonations, NASA SP-273, 1971.

18. McBride, B. J., et. al.: Thermodynamic Properties to 6000°K for 210 Substances Involving the First 18 Elements, NASA SP-3001, 1963.

19. Dash, S. M.; and Del Guidice, P. D.: Analysis of Three-Dimensional Ducted and Exhaust Plume Flowfields, AIAA J., Vol. 16, Aug., 1978, pp 823-830.

20. Abbett, M. J.: Mach Disc in Underexpanded Exhaust Plumes, AIAA J., Vol. 9, March, 1971.

21. Fox, J. H.: On the Structure of Jet Plumes, AIAA J., Vol. 12, Jan., 1974, pp. 105-107.

22. Salas, M. D.: The Numerical Calculation of Inviscid Plume Flowfields, AIAA Paper 74-523, Palo Alto, CA., June, 1974.

23. Dash, S. M.; and Pergament, H. S.: The Analysis of Low Altitude Rocket and Aircraft Plume Flowfields: Modeling Requirements and Procedures, Proceedings of the JANNAF 10th Plume Technology Meeting, CPIA Pub. 291, Vol. I, 1977, pp. 53-132 (Available from DDC as AD B025 704).

24. Pergament, H. S.; Dash, S. M.; and Varma, A. K.: Evaluation of Turbulence Models for Rocket and Aircraft Plume Flowfield Predictions, AIAA Paper No. 79-0359, New Orleans, LA., January, 1979.

25. Patankar, S. W.; and Spalding, D. B.: Heat and Mass Transfer in Boundary Layers, 2nd. Ed., Intertext Books (London), 1970.

26. Jensen, D. E.; and Pergament, H. S.: Effects of Nonequilibrium Chemistry on Electrical Properties of Solid Propellant Rocket Exhaust Plumes, Combustion and Flame, 12, 115 (1971).

27. Wilson, W. E.; and Westenberg, A. A.: Eleventh Symposium (International) on Combustion, The Combustion Institute, Pittsburgh, Pa., 1975, p. 893.

28. Dash, S. M.; Pearce, B. E.; Pergament, H. S.; and Fishburne, E. S.: The Prediction of Rocket and Aircraft Exhaust Plume Structure: Requirements in IR Radiation Signature Studies, AIAA Paper No. 79-0095, New Orleans, La., January, 1979.

29. Dash, S. M.; Pearce, B. E.; Pergament, H. S., and Fishburne, E. S.: On the Prediction of Rocket Plume Flowfields for IR Signature Studies, to be published in Journal of Spacecraft and Rockets, May/June, 1980.

30. anon., Free Turbulent Shear Flows, Vols. I and II, NASA SP-321, July, 1972.

31. Pergament, H. S.; Dash, S. M.; and Fishburne, E. S.: Methodology for the Evaluation of Turbulence Models for Afterburning Rocket and Aircraft Plumes, Proceedings of the JANNAF 10th Plume Technology Meeting, CPIA Pub. 291, Vol. I, 1977, pp. 133-172 (Available from DDC as AD B025 704).

32. Donaldson, C. duP.; and Gray, K. E.: Theoretical and Experimental Investigation of the Compressible Free Mixing of Two Dissimilar Gases, AIAA J., Vol. 4, 1966, pp. 2017-2025.

33. Launder, B. E.; Morse, A.; Rodi, W.; and Spalding, D. B.: Prediction of Free Shear Flows: A Comparison of Six Turbulence Models, in Free Turbulent Shear Flows, Vol. I, NASA SP-321, July, 1972, pp. 361-426.

34. Dash, S. M.; Weilerstein, G.; and Vaglio-Laurin, R.: Compressibility Effects in Free Turbulent Shear Flows, Air Force Office of Scientific Research, TR-75-1436, August, 1975.

35. Kent, J. H.; and Bilger, R. W.: Turbulent Diffusion Flames, TN F-37, Dept. Mech. Eng., University of Sydney, Australia, October, 1972.

36. Evans, J. S.; Schexnayder, C. J.; and Beach, H. L.: Application of Two-Dimensional Parabolic Computer Program to Prediction of Turbulent Reacting Flows, NASA TP-1169, March, 1978.

37. Nelius, M. A.; Darlington, C. R.; and Wasson, R. A.: Exhaust Plume Gas Dynamic and Radiation Measurements on a 500-lbf-Thrust Liquid Rocket Engine, Part I, AEDC TR-77-44, July, 1977. (Available from DDC as AD B020 478L).

TABLE 1

Summary of Constant Pressure, Turbulent Shear Flow
Comparisons of BOAT Predictions with Laboratory Data

Case Description	Data Description	Turbulence Models Used*	References
1) 2D incompressible shear layers with variable velocity ratios	Test Case 1 of NASA Shear Flow Conference - (various data)	ML; kε2	6, 8, 9, 31
2) 2D compressible shear layers	Test Case 2 of NASA Shear Flow Conference - (various data)	ML; D/G; kε2; kε2, cc	24, 31
3) 2D incompressible shear layers with initial boundary layers	Test Case 4 of NASA Shear Flow Conference - Lee and Childs data	ML; kε2	6, 8, 9, 31
4) Axisymmetric jet into still air ($M_j \sim .6$)	Test Case 6 of NASA Shear Flow Conference - Maestrello and McDaid data	ML; D/G; kε2	24
5) Axisymmetric jet into still air (low speed jet)	Test Case 18 of NASA Shear Flow Conference - Wygnanski and Fiedler data	ML; D/G; kε2	24, 31
6) Axisymmetric jet into still air ($M_J = 2.22$)	Test Case 7 of NASA Shear Flow Conference - Eggers data	ML; D/G; kε2; kε2, cc	24, 31
7) Axisymmetric jet into moving stream ($M_J/M_E = .10/.03$)	Test Case 9 of NASA Shear Flow Conference - Forstall and Shapiro data	ML; D/G; kε2	6, 8, 9, 24
8) Hydrogen jet into moving stream ($M_J/M_E = .89/1.32$	Test Case 12 of NASA Shear Flow Conference - Eggers data	ML; D/G; kε2, cc	24
9) H_2/air diffusion flame	Kent and Bilger data[35]	D/G; kε2	24
10) Reacting hydrogen jet into moving stream ($M_J/M_E = 2.0/1.9$)	Beach data[36]	ML; D/G; kε2; kε2, cc	24
11) Afterburning plume from 227 kg thrust amine-fueled rocket motor ($M_J/M_E = 3.5/2.0$)	AEDC data[37]	kε2; kε2, cc	24

*ML - extended mixing length model (Ref. 6)
D/G - Donaldson/Gray eddy viscosity model (Ref. 32)
kε2 - two-equation turbulence model (Ref. 33)
kε2, cc - compressibility corrected two-equation turbulence model (Ref. 34)

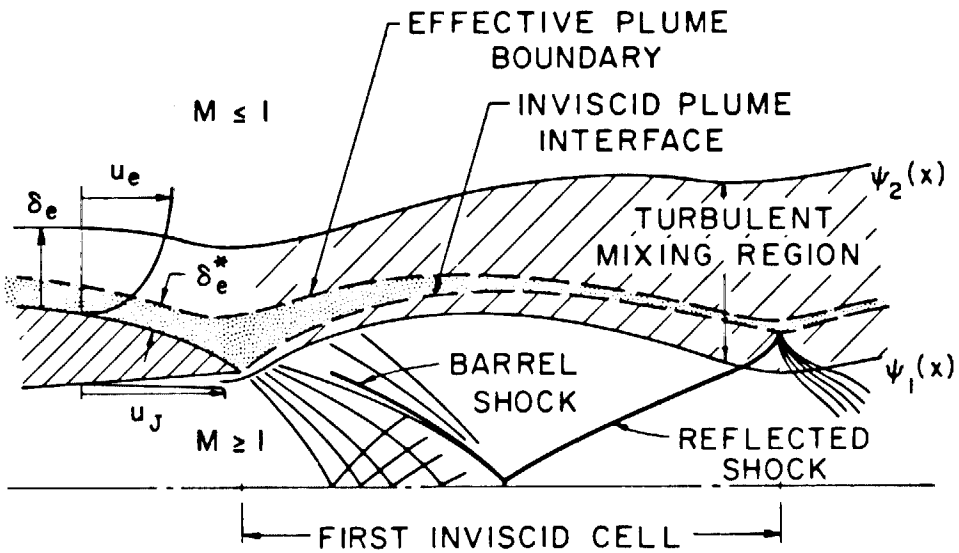

Figure 1. Schematic of afterbody/exhaust flowfield

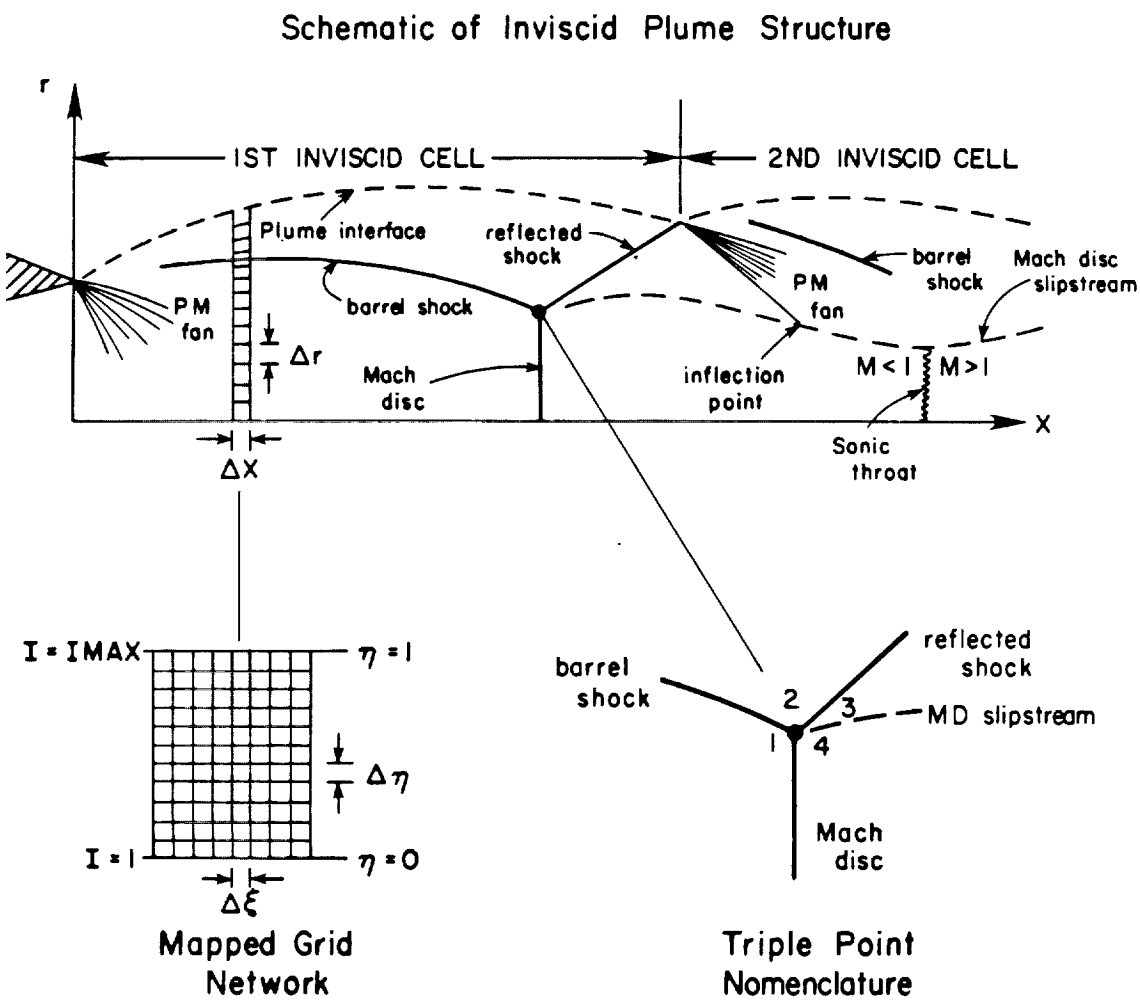

Figure 2. Inviscid exhaust plume structure

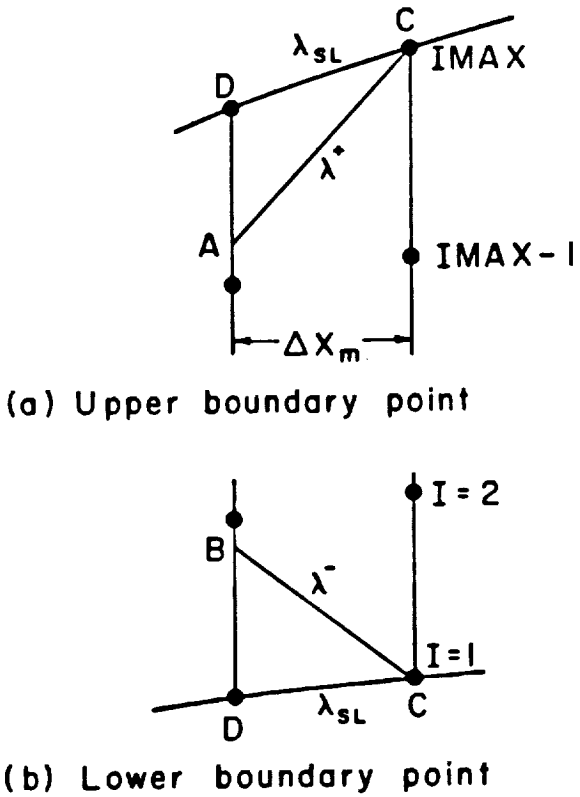

Figure 3. Characteristic nomenclature at boundary points

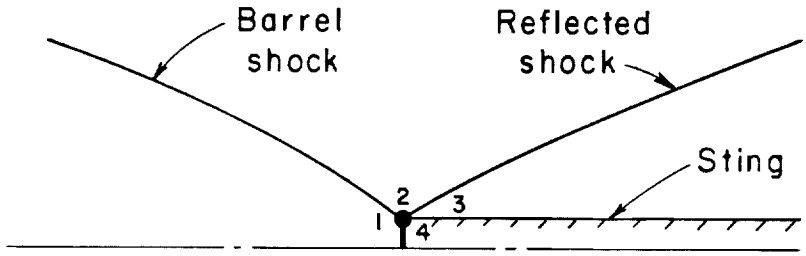

(a) Sting approach for small Mach discs

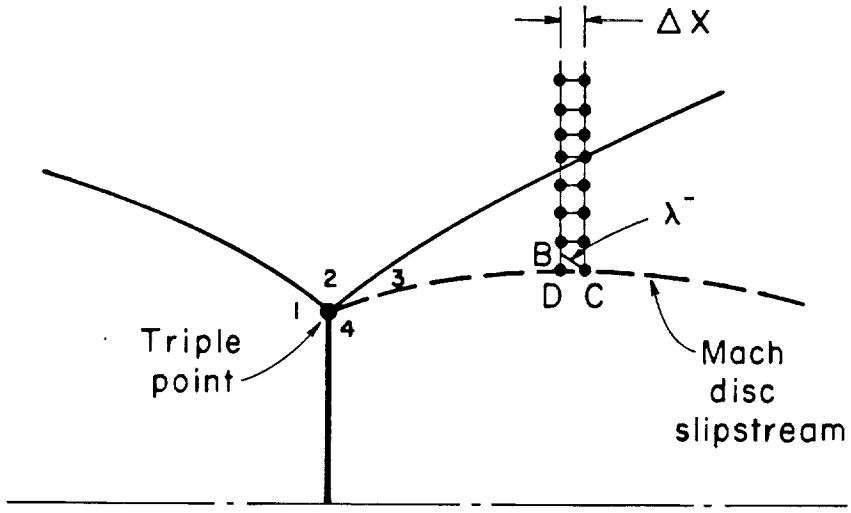

(b) Abbett approach for large Mach discs

Figure 4. Mach disc nomenclature

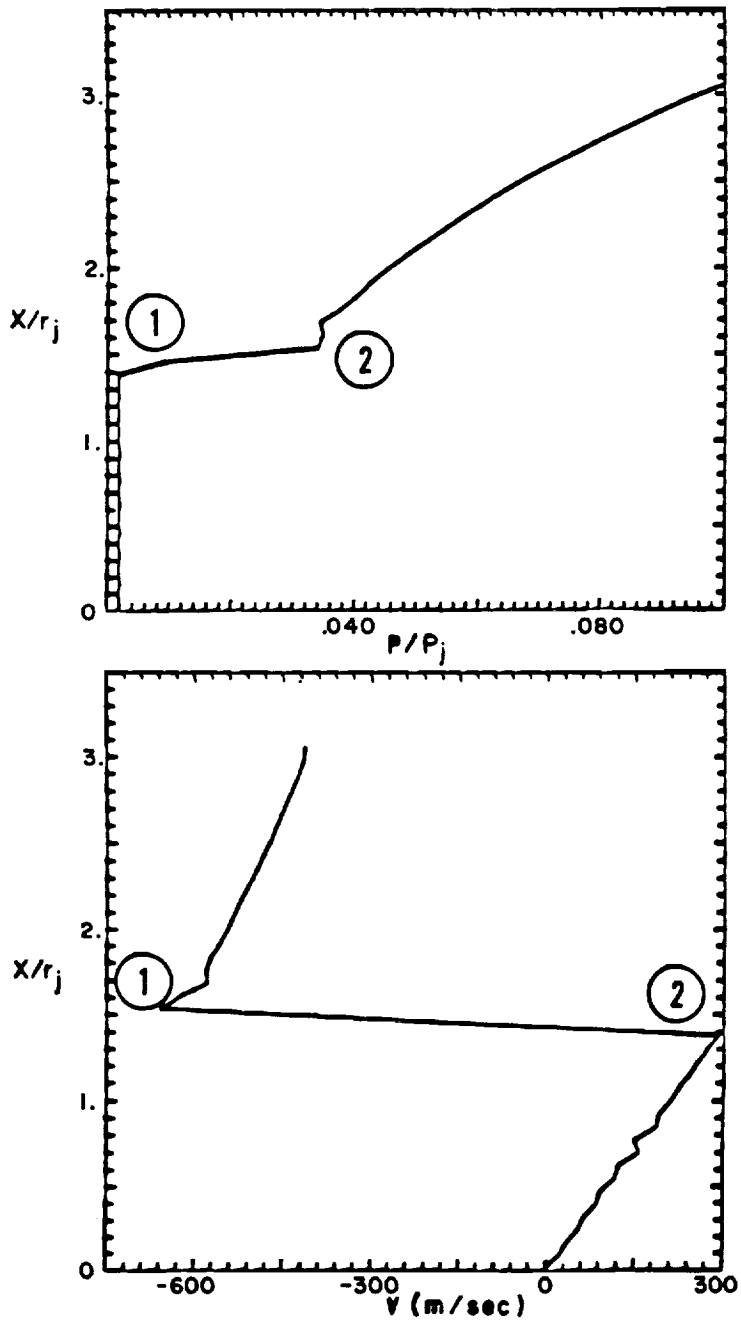

Figure 5. Pressure and normal velocity profiles showing captured barrel shock

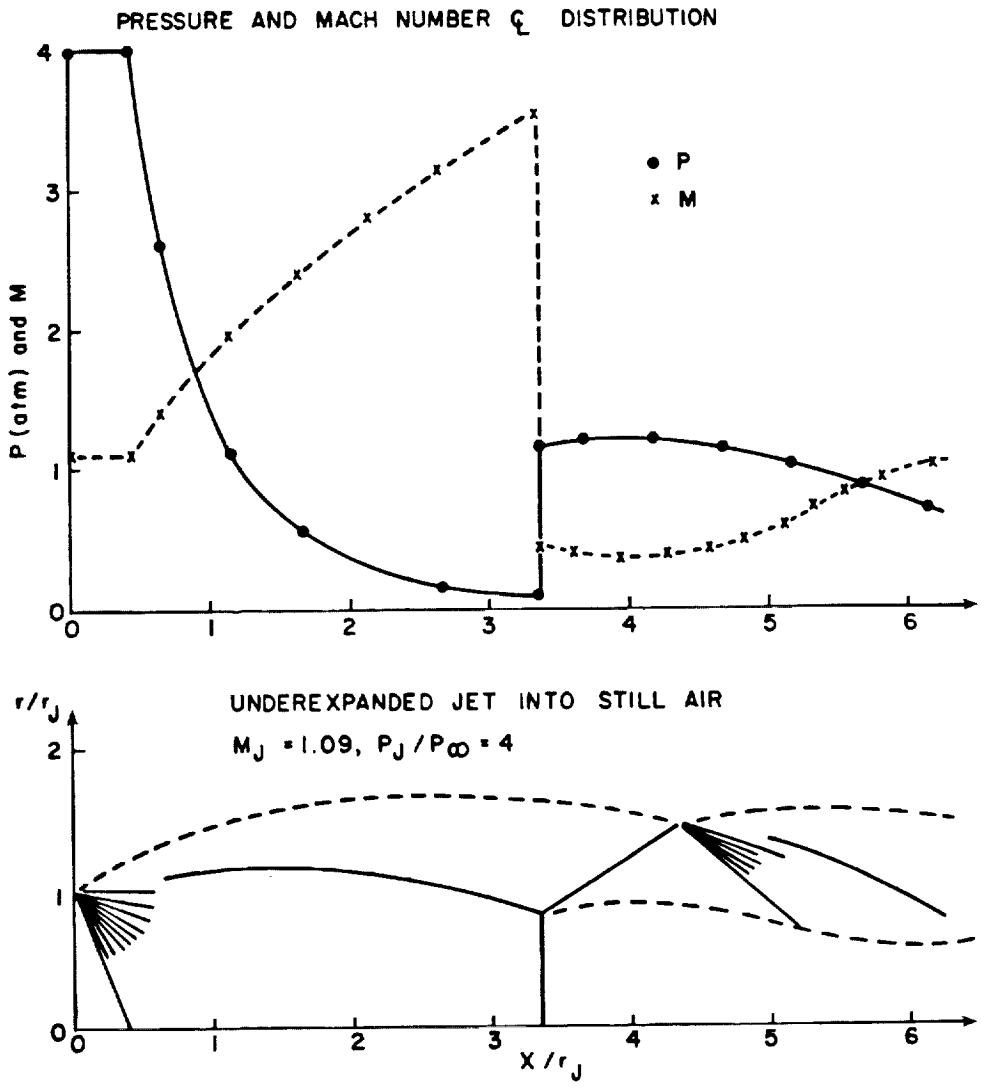

Figure 6. Flowfield schematic of underexpanded hot air jet and predicted centerline pressure and Mach number variation

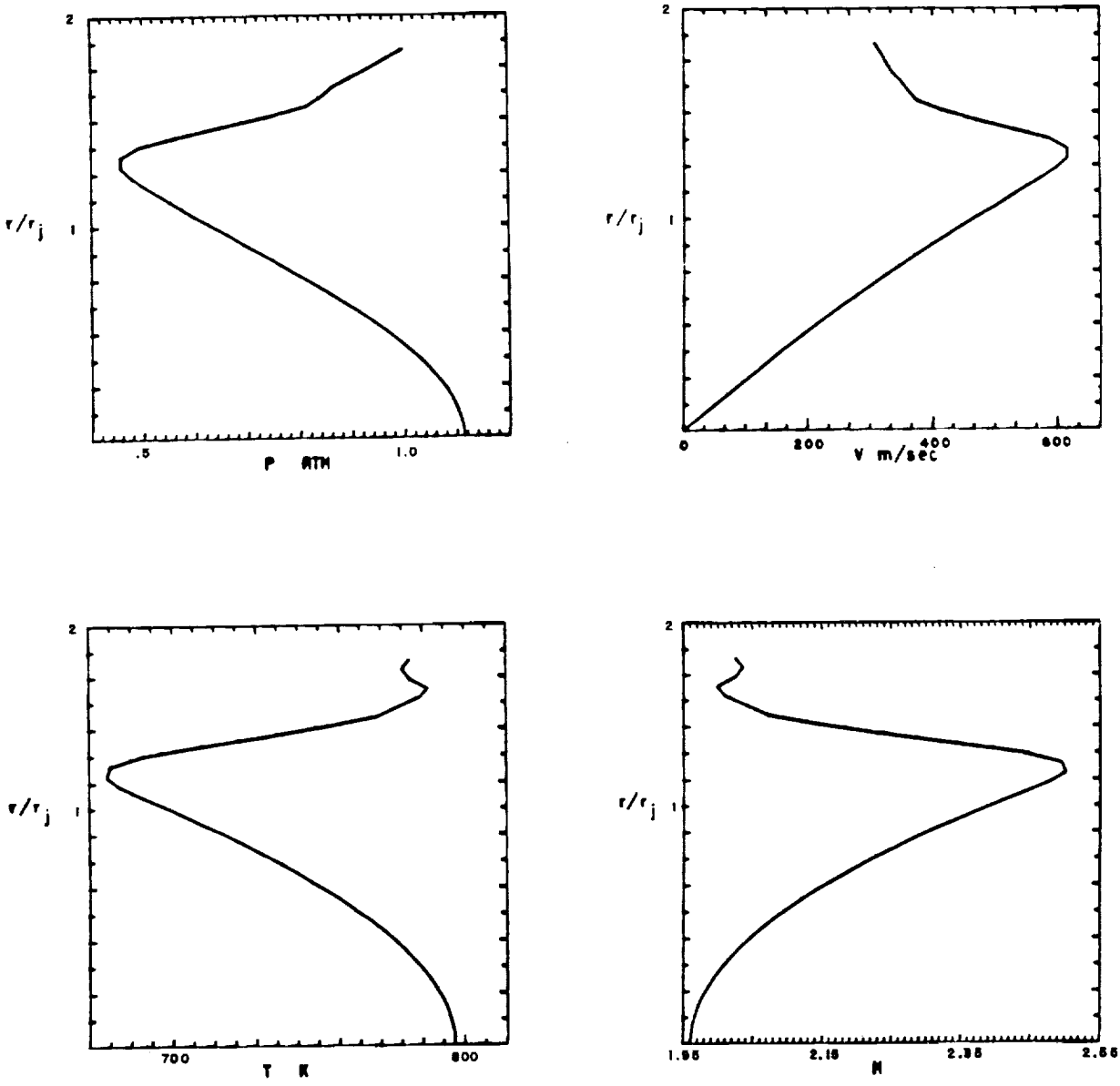

Figure 7A. Profiles of P, V, T and M at $X/r_j = 1.16$

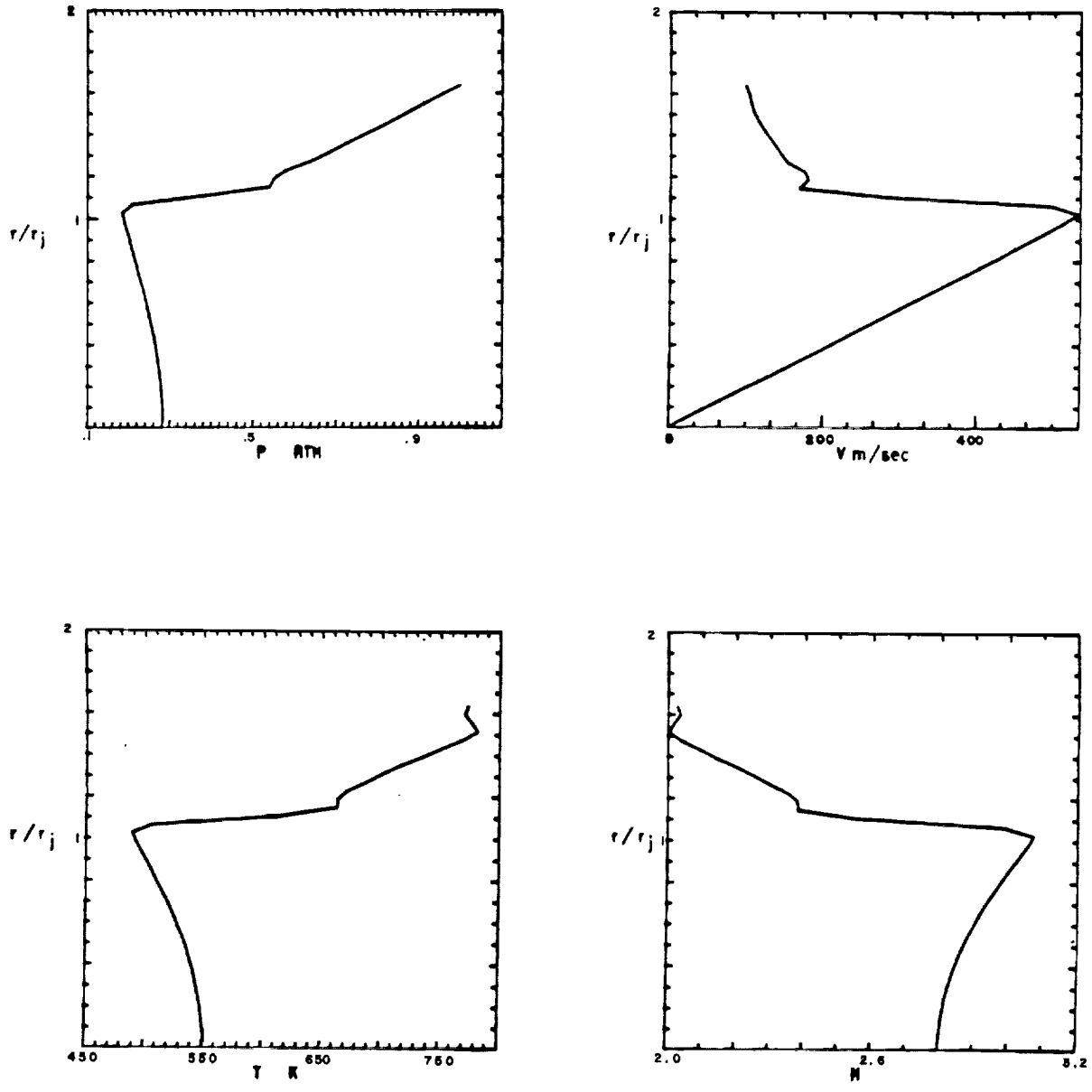

Figure 7B. Profiles at 2.17

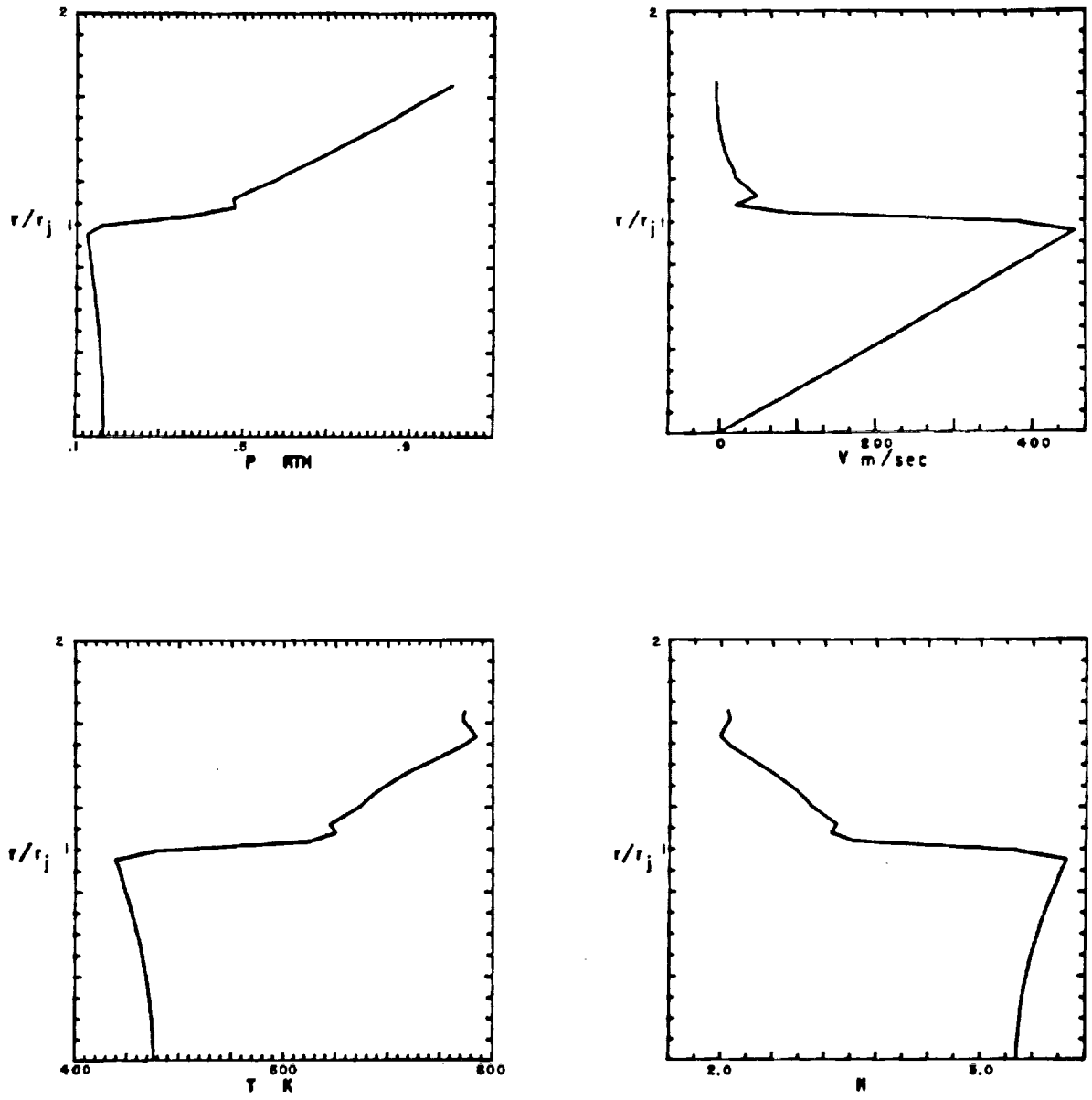

Figure 7C. Profiles at 2.67

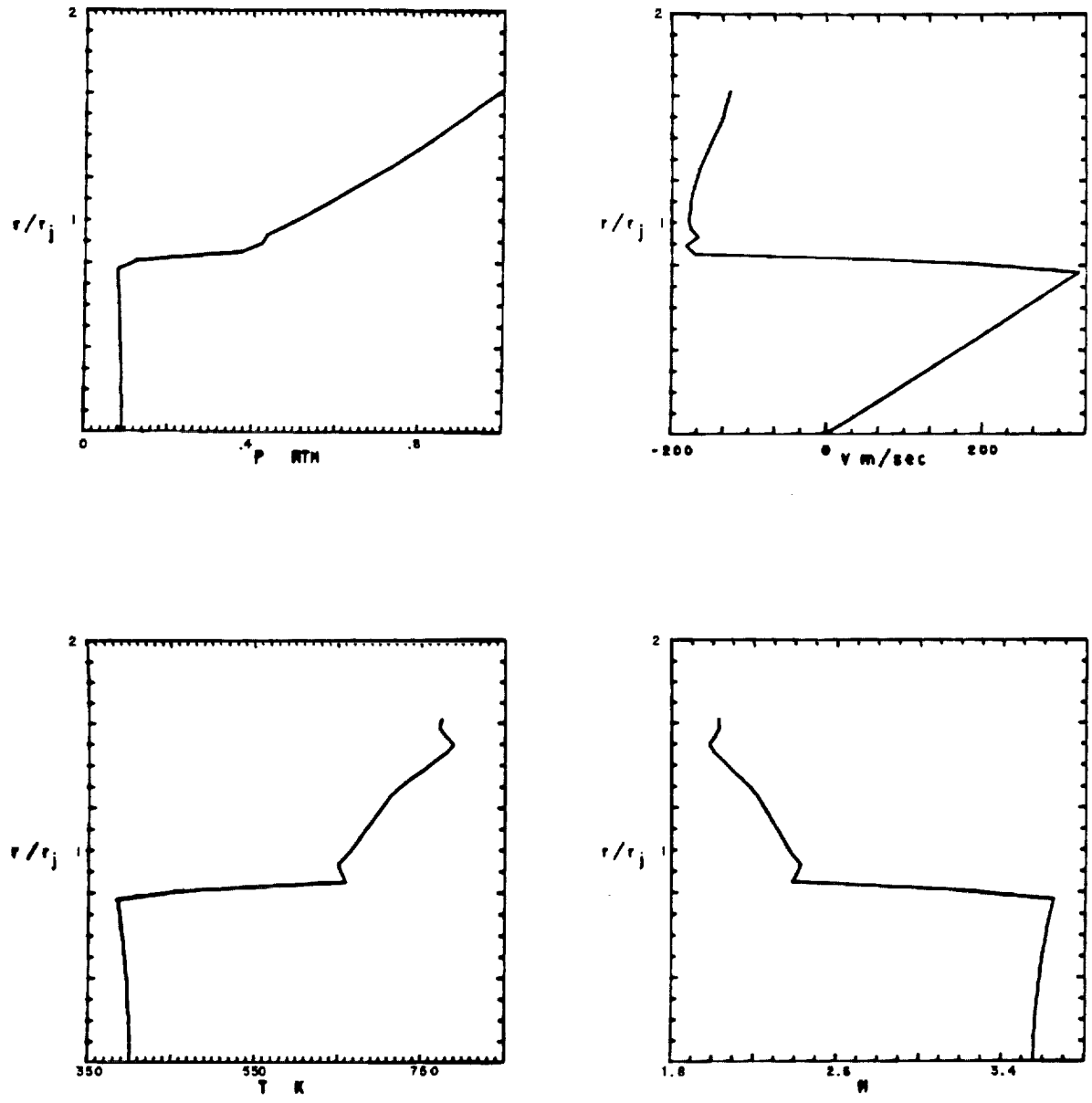

Figure 7D. Profiles at 3.35, upstream of Mach disc

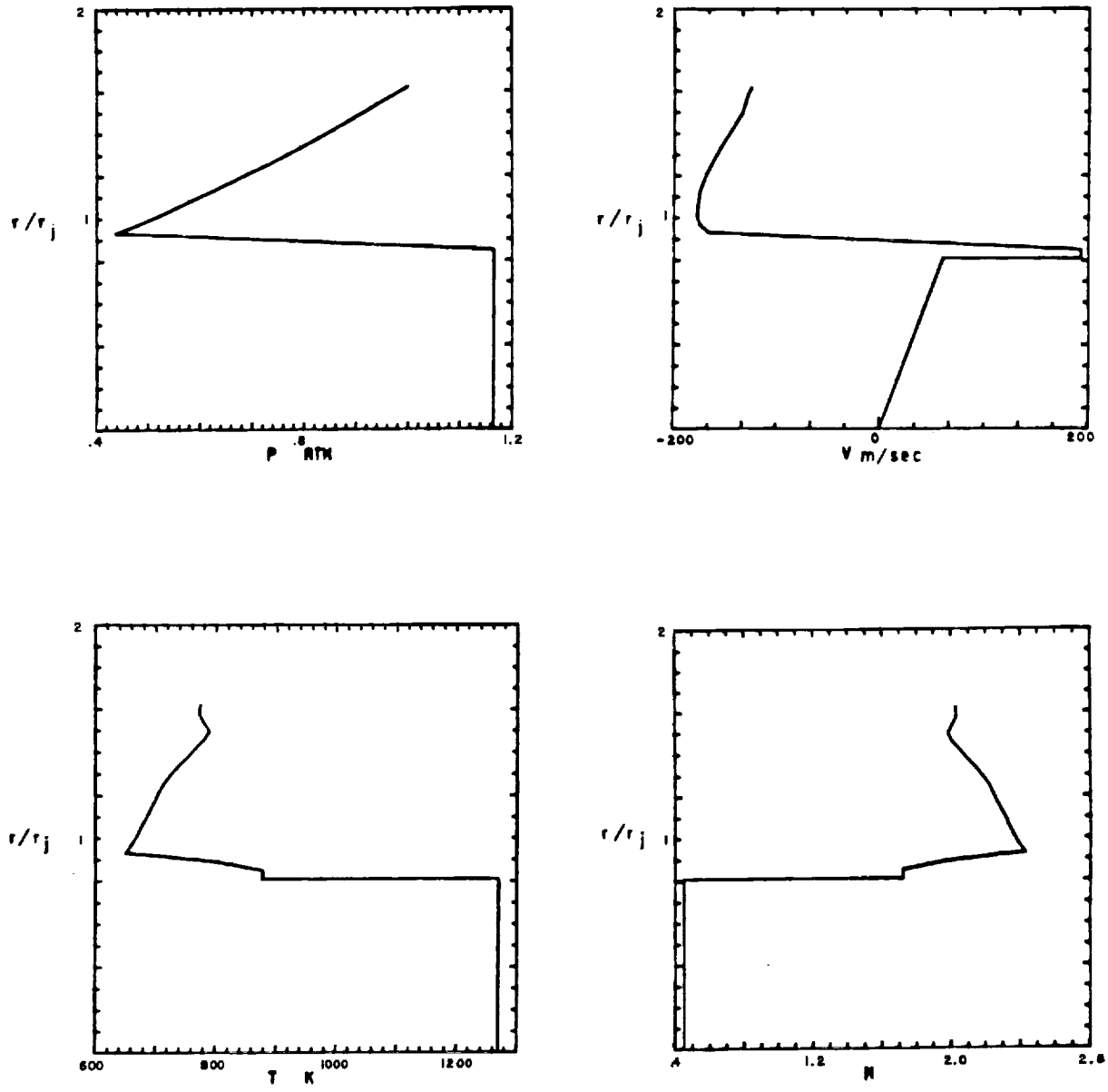

Figure 7E. Profiles at 3.35, downstream of Mach disc

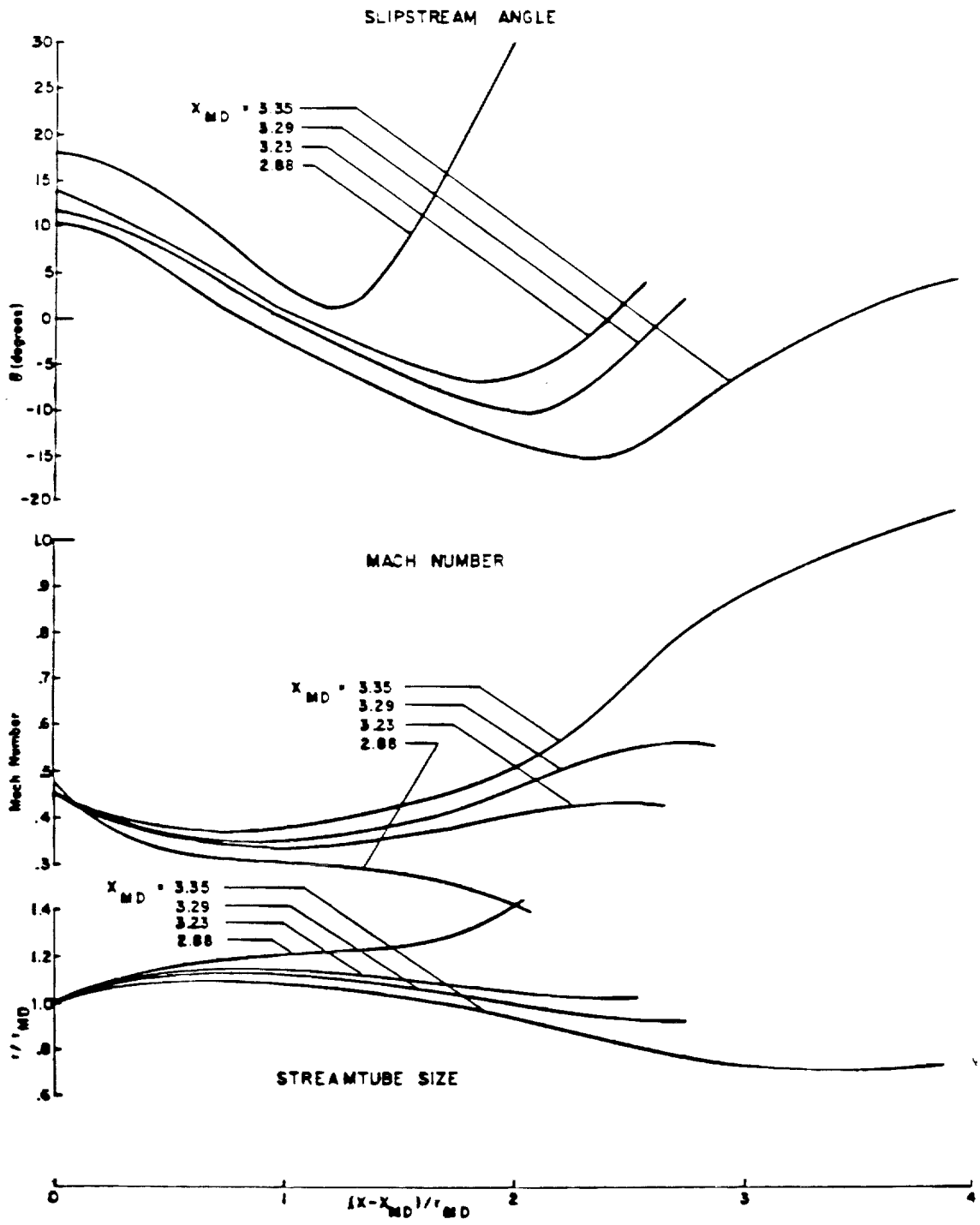

Figure 8. Axial variations of Mach number, slipstream angle and streamtube size for several trial Mach disc locations

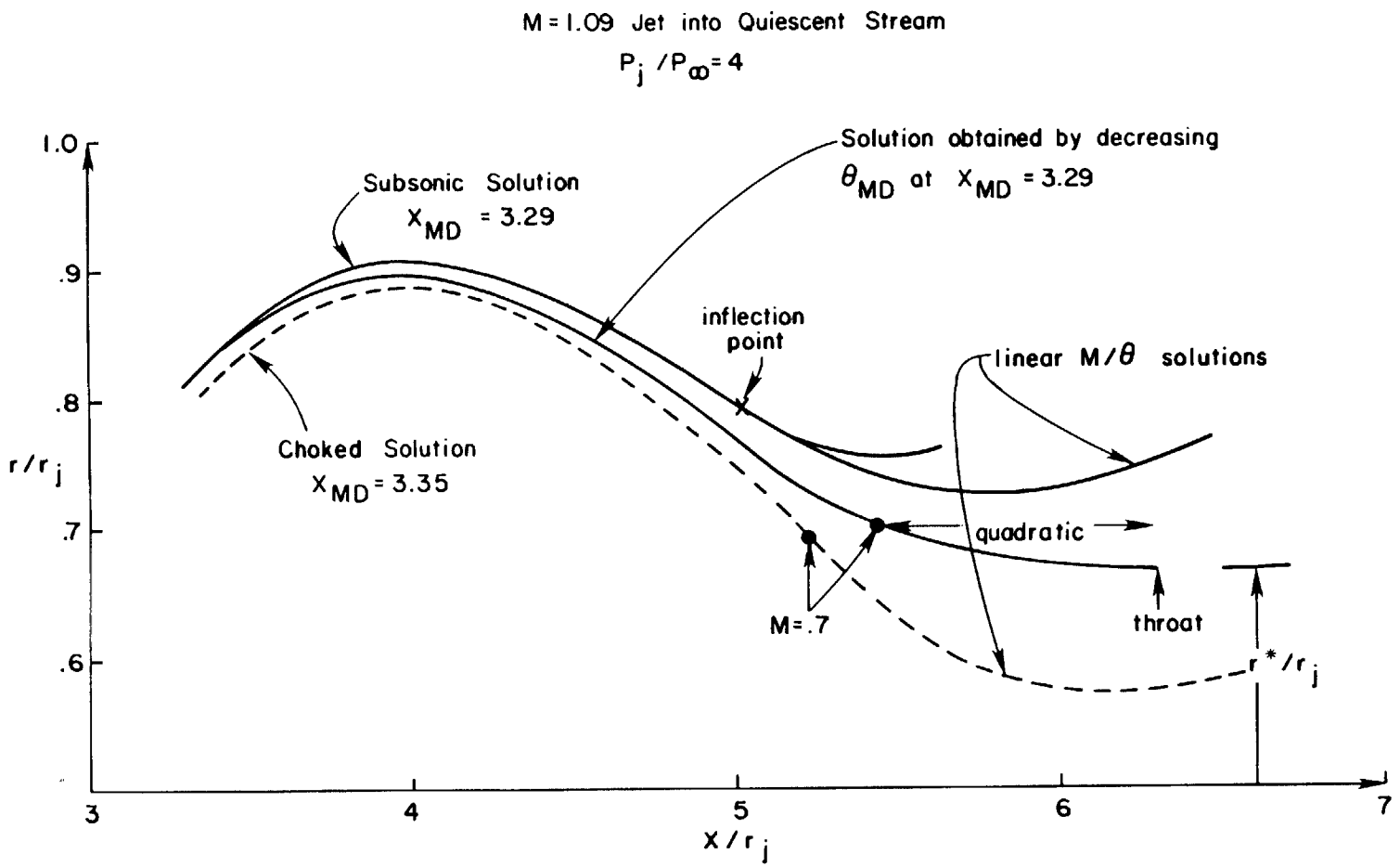

Figure 9. Comparison of several techniques for getting through the throat

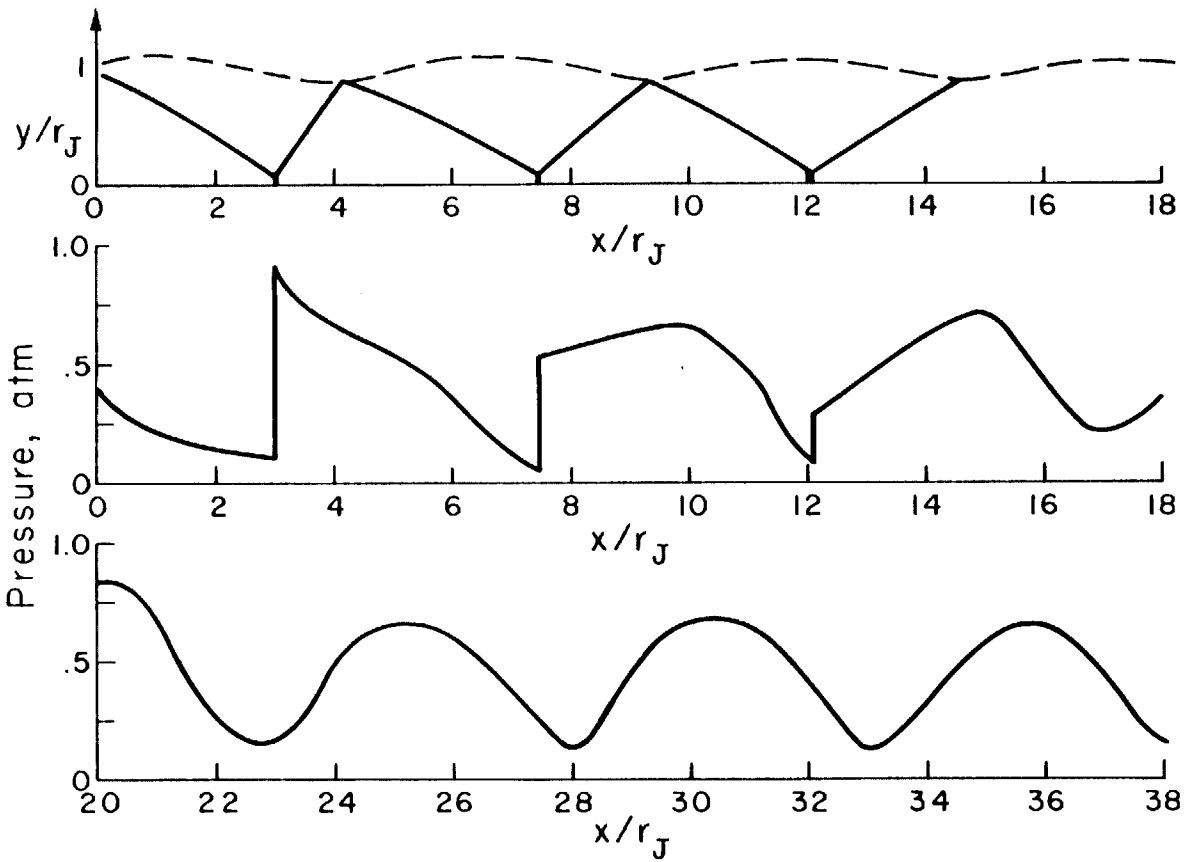

Figure 10. Multiple cell inviscid pattern for slightly overexpanded plume exhausting into still air

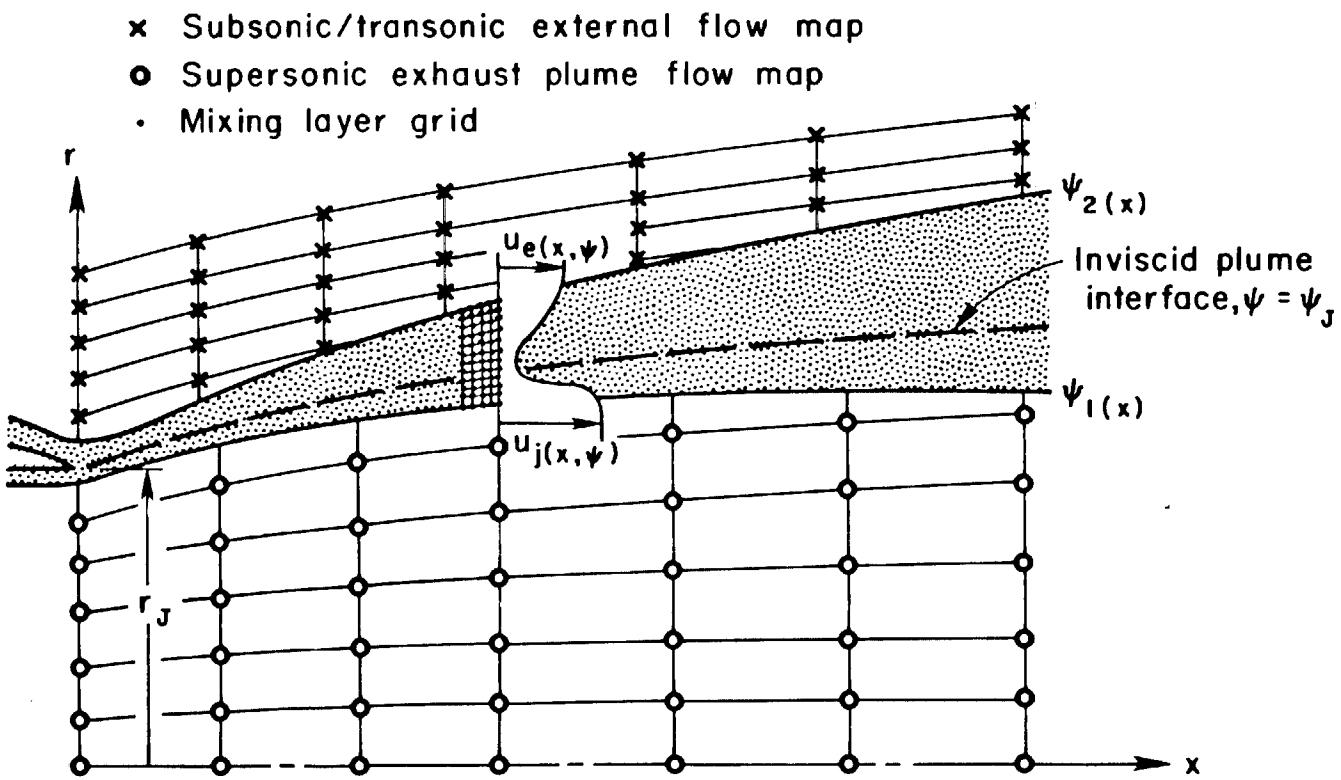

Figure 11. Mixing solution overlaid on inviscid flowfield maps

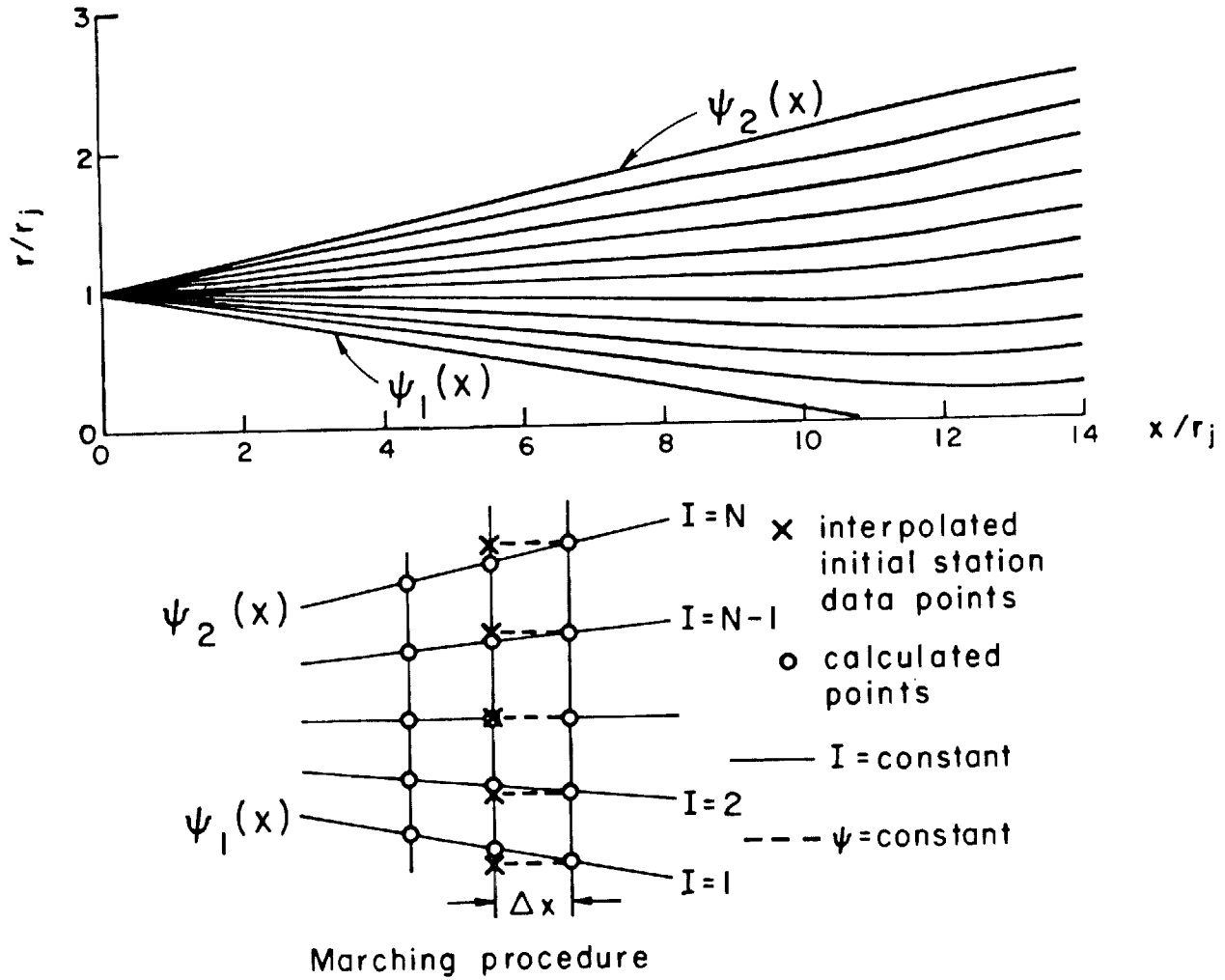

Figure 12. Computational network of BOAT

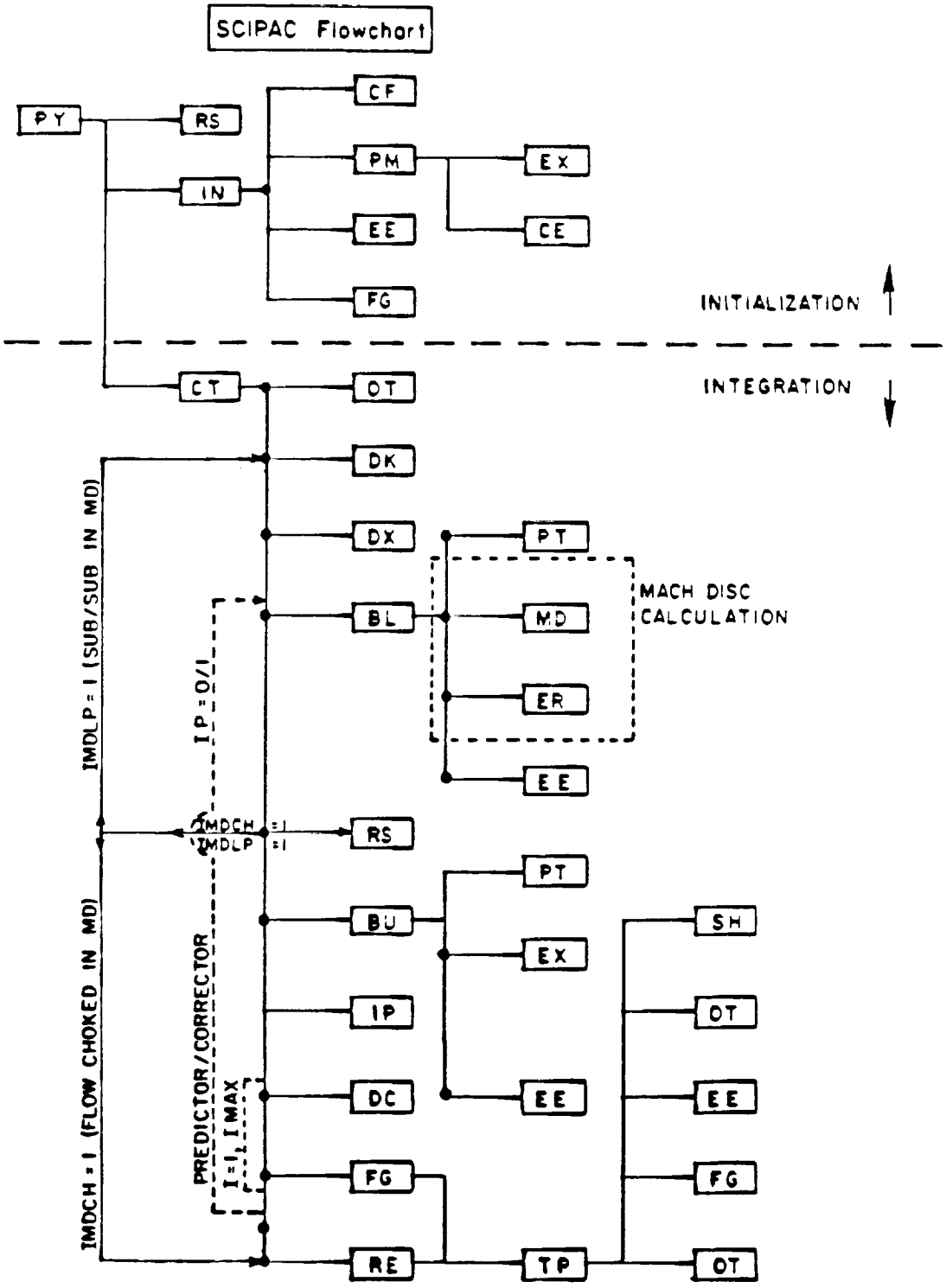

Figure 13. SCIPAC subroutine flowchart

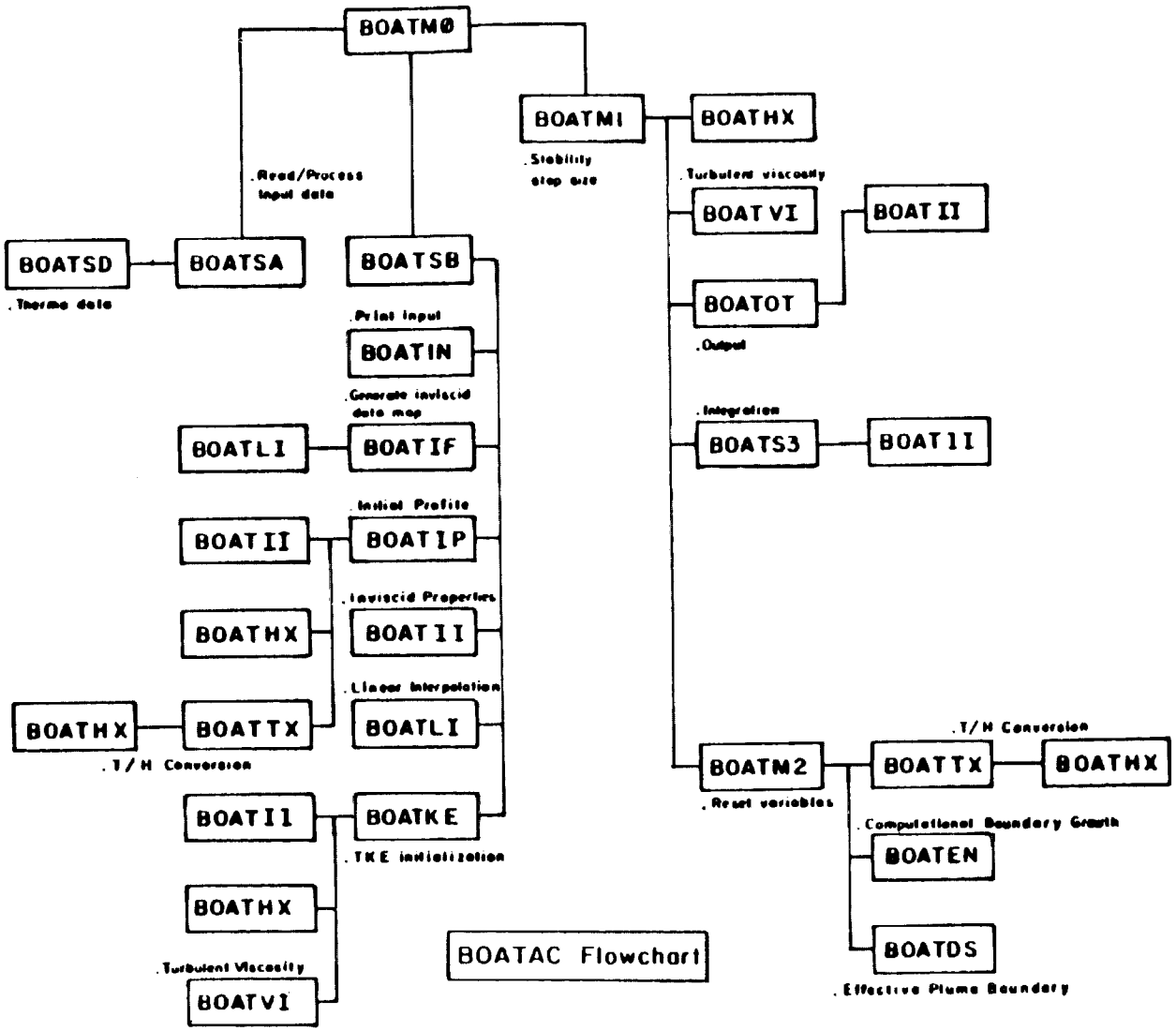

Figure 14. BOATAC subroutine flowchart

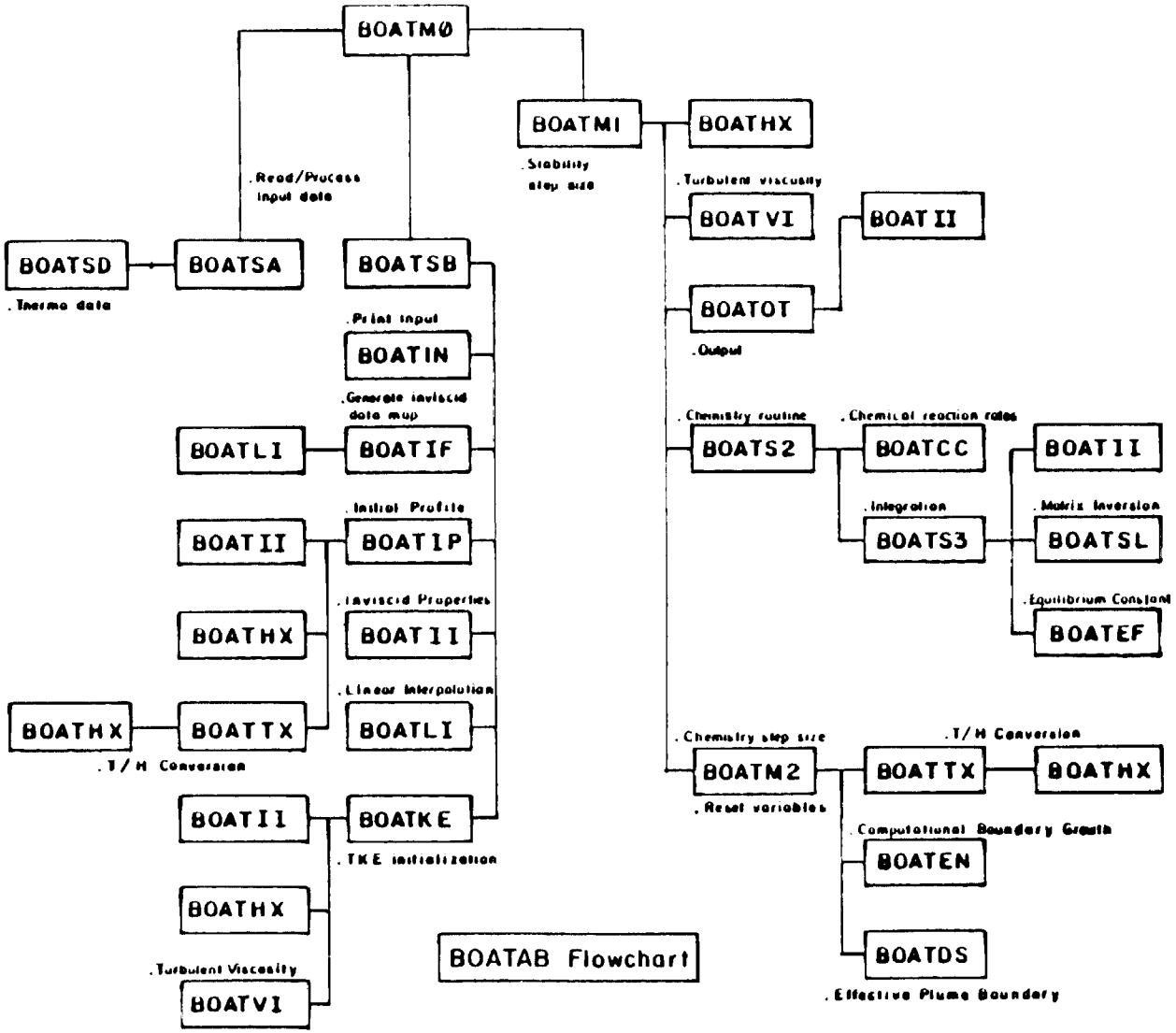

Figure 15. BOATAB subroutine flowchart

1. Report No.	2. Government Accession No.	3. Recipient's Catalog No.
NASA CR-3289		

4. Title and Subtitle	5. Report Date
Computational Models for the Viscous/Inviscid Analysis of Jet Aircraft Exhaust Plumes	May 1980
	6. Performing Organization Code

7. Author(s)	8. Performing Organization Report No.
Sanford M. Dash, Harold S. Pergament, and Roger D. Thorpe	A.R.A.P. 408
	10. Work Unit No. 505-32-13-01

9. Performing Organization Name and Address	11. Contract or Grant No.
Aeronautical Research Associates of Princeton, Inc. 50 Washington Road Princeton, NJ 08540	NAS1-14794
	13. Type of Report and Period Covered: Contractor Report

12. Sponsoring Agency Name and Address	14. Sponsoring Agency Code
National Aeronautics and Space Administration Washington, D.C. 20546	

15. Supplementary Notes

Langley Technical Monitor: Richard G. Wilmoth
Final Report

16. Abstract

Computational models which analyze viscous/inviscid flow processes in jet aircraft exhaust plumes are discussed. These models are component parts of an NASA-LaRC method for the prediction of nozzle afterbody drag. Inviscid/shock processes are analyzed by the SCIPAC code which is a compact version of a generalized shock-capturing, inviscid plume code (SCIPPY). SCIPAC analyzes underexpanded jet exhaust gas mixtures with a self-contained thermodynamic package for hydrocarbon exhaust products and air. A detailed and automated treatment of the embedded subsonic zones behind Mach discs is provided in this analysis. Mixing processes along the plume interface are analyzed by two upgraded versions of an overlaid, turbulent mixing code (BOAT) developed previously for calculating nearfield jet entrainment. BOATAC is a frozen chemistry version of BOAT containing the same aircraft thermodynamic package as SCIPAC. BOATAB is an afterburning version with a self-contained aircraft (hydrocarbon/air) finite-rate chemistry package. The coupling of viscous and inviscid flow processes is achieved by an overlaid procedure with interactive effects accounted for by a displacement thickness type correction to the inviscid plume interface.

17. Key Words (Suggested by Author(s))	18. Distribution Statement
Jet Aircraft Plumes Underexpanded Jets Turbulent Mixing Jet Entrainment Viscous/Inviscid Interactions	Unclassified - Unlimited Subject Category 34

19. Security Classif. (of this report)	20. Security Classif. (of this page)	21. No. of Pages	22. Price*
Unclassified	Unclassified	77	$6.00

For sale by the National Technical Information Service, Springfield, Virginia 22161

NASA-Langley, 1980